Discovery prospects for NMSSM Higgs bosons at the high-energy Large Hadron Collider

S. F. King,[1,*] M. Mühlleitner,[2,†] R. Nevzorov,[3,‡] and K. Walz[2,§]

[1]*School of Physics and Astronomy, University of Southampton, Southampton SO17 1BJ, United Kingdom*
[2]*Institute for Theoretical Physics, Karlsruhe Institute of Technology, 76128 Karlsruhe, Germany*
[3]*ARC Centre of Excellence for Particle Physics at the Tera-scale, School of Chemistry and Physics, University of Adelaide, Adelaide, South Australia 5005, Australia*

(Received 22 August 2014; published 14 November 2014)

We investigate the discovery prospects for Higgs bosons in the next-to-mininmal supersymmetric extension of the Standard Model (NMSSM) during the 13 TeV run of the LHC. While one of the neutral Higgs bosons is demanded to have a mass around 125 GeV and Standard Model-like properties, there can be substantially lighter, nearby or heavier Higgs bosons that have not been excluded yet by LEP, Tevatron or the 8 TeV run of the LHC. The challenge consists in discovering the whole NMSSM Higgs mass spectrum. We present the rates for production and subsequent decay of the neutral NMSSM Higgs bosons in the most promising final states and discuss their possible discovery. The prospects for pinning down the Higgs sector of the natural NMSSM will be analyzed taking into account alternative search channels. We give a series of benchmark scenarios compatible with the experimental constraints, that feature Higgs-to-Higgs decays and entail (exotic) signatures with multifermion and/or multiphoton final states. These decay chains furthermore give access to the trilinear Higgs self-couplings. We briefly discuss the possibility of exploiting coupling sum rules in case not all the NMSSM Higgs bosons are discovered.

DOI: 10.1103/PhysRevD.90.095014 PACS numbers: 12.60.Jv, 12.60.-i, 12.60.Fr, 14.80.Da

I. INTRODUCTION

The discovery of a new particle with mass around 125 GeV by the Large Hadron Collider Experiments ATLAS and CMS [1,2] has immediately triggered investigations of its properties such as spin and CP quantum numbers and couplings to other Standard Model (SM) particles. These analyses conclude so far that the discovered particle is a Higgs boson which behaves rather SM-like. Additionally no new resonances have been discovered which could point to extensions beyond the SM (BSM). This renders the detailed investigation of the Higgs properties at highest possible accuracy accompanied by the search for new particles even more important. The Higgs sector of supersymmetric extensions of the SM introduces an enlarged Higgs spectrum due to the requirement of at least two complex Higgs doublets to ensure supersymmetry (SUSY) [3]. These lead in the minimal supersymmetric extension of the SM (MSSM) [4] to five Higgs bosons. The next-to-minimal supersymmetric extension of the SM (NMSSM) [5] is extended by an additional complex superfield $\hat{S}$ and allows for a dynamical solution of the μ problem [6] when the singlet field acquires a non-vanishing vacuum expectation value. After electroweak symmetry breaking (EWSB) the NMSSM Higgs sector features seven Higgs bosons, which are in the CP-conserving case given by three neutral CP-even, two neutral CP-odd and two charged Higgs bosons. A nice consequence of the singlet superfield, which couples to the Higgs doublet superfields $\hat{H}_u$ and $\hat{H}_d$, are new contributions to the quartic coupling proportional to the singlet-doublet coupling λ so that the tree-level mass value of the lighter MSSM-like Higgs boson is increased. Therefore less important radiative corrections are required to shift the mass value to 125 GeV and in turn smaller stop masses and/or mixing, allowing for less fine-tuning [7,8].

The singlet admixture in the Higgs mass eigenstates entails reduced couplings to the SM particles. Together with the enlarged Higgs sector this leads to a plethora of interesting phenomenological scenarios and signatures. Thus very light Higgs bosons are not yet excluded by the LEP searches [9] if their SM couplings are small enough. In turn heavier Higgs bosons can decay into a pair of lighter Higgs bosons subsequently decaying into SM particles which leads to interesting final state signatures [10–12]. Furthermore, branching ratios into LHC standard search channels such as $\gamma\gamma$ or vector boson final states can be enhanced or suppressed [8,13]. An enhanced photonic rate of the 125 GeV Higgs boson can also be due to two almost degenerate Higgs bosons with masses near 125 GeV [8,14]. The investigation of double ratios of signal rates at the high-energy option of the LHC would allow for the resolution of the double peak [15]. It is obvious that on the theoretical side the reliable interpretation of such BSM signatures and the disentanglement of different SUSY

*king@soton.ac.uk
†margarete.muehlleitner@kit.edu
‡roman.nevzorov@adelaide.edu.au
§kathrin.walz@kit.edu

scenarios as well as their distinction from the SM situation requires precise predictions of the SUSY parameters such as masses and Higgs couplings to other Higgs bosons including higher order corrections. For the CP-conserving NMSSM the mass corrections are available at one-loop accuracy [16–20], and two loop results of $\mathcal{O}(\alpha_t\alpha_s + \alpha_b\alpha_s)$ in the approximation of zero external momentum have been given in Ref. [18]. In the complex case the Higgs mass corrections have been calculated at one-loop accuracy [21–24] with the logarithmically enhanced two-loop effects given in [25]. Higher-order corrections to the trilinear Higgs self-coupling of the neutral NMSSM Higgs bosons have been provided in [10]. But also constraints that arise from dark matter, the low-energy observables, the direct Higgs boson searches at LEP, Tevatron and the LHC as well as restrictions on the SUSY parameter space due to the exclusion bounds on SUSY particle masses have to be included when investigating viable NMSSM scenarios. By performing a scan over wide ranges of the NMSSM parameter space, incorporating in our analysis higher-order corrections to the NMSSM Higgs parameters and their production and decay rates [26–28] and taking into account experimental constraints, we investigate the features of the NMSSM Higgs spectrum, the Higgs mass values and mixings.[1] We present signal rates for the various SM final states and discuss the prospect of discovering the NMSSM Higgs bosons during the next run of the LHC at a center-of-mass (c.m.) energy of 13 TeV. Subsequently, we restrict ourselves to a subspace of the NMSSM with a slightly broken Peccei-Quinn symmetry, that is characterized by a rather light Higgs spectrum with masses below about 530 GeV. This subspace, which we call natural NMSSM, turns out to allow for the discovery of all Higgs bosons for a large fraction of its scenarios. It can therefore be tested or ruled out at the next LHC run. Besides their direct production, the Higgs bosons can also be produced in the decays of heavier Higgs bosons into lighter Higgs pairs or into a Higgs and gauge boson pair. The Higgs-to-Higgs decay processes give access to the trilinear Higgs self-couplings, which are a necessary ingredient for the reconstruction and test of the Higgs potential. We present benchmark scenarios that cover various aspects of Higgs-to-Higgs decays. We find that they lead to, in part unique, in part exotic, multiphoton and/or multilepton final states. These scenarios can therefore be viewed as benchmark scenarios and should be considered in the experimental searches to make sure that no BSM states will be missed. We also briefly discuss what can be learned from the couplings of the discovered Higgs bosons in case not all of the NMSSM Higgs bosons are accessible.

The layout of the remainder of this paper is as follows. In Sec. II we briefly introduce the NMSSM Lagrangian. In Sec. III the details of the scan in the NMSSM parameter space are given. Our results are shown in Sec. IV. After presenting the parameter and mass distributions in subsections IV A and IV B, the NMSSM Higgs signal rates in various final states will be discussed in subsection IV C. Section V is devoted to the analysis of the natural NMSSM. In Section VI we present several benchmark scenarios that feature Higgs-to-Higgs decays. Section VII summarizes and concludes the paper.

[1]For recent studies on the NMSSM phenomenology, see [29–44].

II. THE NMSSM LAGRANGIAN

The NMSSM differs from the MSSM in the superpotential and the soft SUSY breaking Lagrangian. In terms of the (hatted) superfields and including only the third generation fermions, the scale invariant NMSSM superpotential reads

$$\mathcal{W} = \lambda\hat{S}\hat{H}_u\hat{H}_d + \frac{\kappa}{3}\hat{S}^3 + h_t\hat{Q}_3\hat{H}_u\hat{t}^c_R - h_b\hat{Q}_3\hat{H}_d\hat{b}^c_R - h_\tau\hat{L}_3\hat{H}_d\hat{\tau}^c_R. \tag{2.1}$$

The first term replaces the μ-term $\mu\hat{H}_u\hat{H}_d$ of the MSSM superpotential. The second term, which is cubic in the singlet superfield, breaks the Peccei-Quinn symmetry [45], so that no massless axion can appear. The last three terms are the Yukawa interactions. The soft SUSY breaking Lagrangian receives contributions from the scalar mass parameters for the Higgs and sfermion fields, which in terms of the fields corresponding to the complex scalar components of the superfields read

$$-\mathcal{L}_{\text{mass}} = m^2_{H_u}|H_u|^2 + m^2_{H_d}|H_d|^2 + m^2_S|S|^2 + m^2_{\tilde{Q}_3}|\tilde{Q}^2_3| + m^2_{\tilde{t}_R}|\tilde{t}^2_R| + m^2_{\tilde{b}_R}|\tilde{b}^2_R| + m^2_{\tilde{L}_3}|\tilde{L}^2_3| + m^2_{\tilde{\tau}_R}|\tilde{\tau}^2_R|. \tag{2.2}$$

The Lagrangian including the trilinear soft SUSY breaking interactions between the sfermions and Higgs fields is given by

$$-\mathcal{L}_{\text{tril}} = \lambda A_\lambda H_u H_d S + \frac{1}{3}\kappa A_\kappa S^3 + h_t A_t \tilde{Q}_3 H_u \tilde{t}^c_R - h_b A_b \tilde{Q}_3 H_d \tilde{b}^c_R - h_\tau A_\tau \tilde{L}_3 H_d \tilde{\tau}^c_R + \text{h.c.} \tag{2.3}$$

The soft SUSY breaking Lagrangian with the gaugino mass parameters finally reads

$$-\mathcal{L}_{\text{gauginos}} = \frac{1}{2}\left[M_1\tilde{B}\,\tilde{B} + M_2\sum_{a=1}^{3}\tilde{W}^a\tilde{W}_a + M_3\sum_{a=1}^{8}\tilde{G}^a\tilde{G}_a + \text{h.c.}\right]. \tag{2.4}$$

We will work in the unconstrained NMSSM with nonuniversal soft terms at the GUT scale. After EWSB the Higgs

doublet and singlet fields acquire nonvanishing vacuum expectation values (VEVs). The SUSY breaking masses squared for H_u, H_d and S in $\mathcal{L}_{\rm mass}$ are traded for their tadpole parameters by exploiting the three minimisation conditions of the scalar potential.

The NMSSM Higgs potential is obtained from the superpotential, the soft SUSY breaking terms and the D-term contributions. Expanding the Higgs fields about their VEVs v_u, v_d and v_s, which we choose to be real and positive,

$$H_d = \begin{pmatrix} (v_d + h_d + ia_d)/\sqrt{2} \\ h_d^- \end{pmatrix},$$
$$H_u = \begin{pmatrix} h_u^+ \\ (v_u + h_u + ia_u)/\sqrt{2} \end{pmatrix},$$
$$S = \frac{v_s + h_s + ia_s}{\sqrt{2}}, \tag{2.5}$$

the Higgs mass matrices for the three scalar, two pseudoscalar and the charged Higgs bosons are derived from the tree-level scalar potential. The squared 3×3 mass matrix M_S^2 for the CP-even Higgs fields is diagonalized through a rotation matrix $\mathcal{R}^S$ yielding the CP-even mass eigenstates H_i $(i = 1, 2, 3)$,

$$(H_1, H_2, H_3)^T = \mathcal{R}^S (h_d, h_u, h_s)^T, \tag{2.6}$$

with the H_i ordered by ascending mass, $M_{H_1} \leq M_{H_2} \leq M_{H_3}$. The CP-odd mass eigenstates A_1, A_2 and the massless Goldstone boson G are obtained by consecutively applying a rotation $\mathcal{R}^G$ to separate G, followed by a rotation $\mathcal{R}^P$ to obtain the mass eigenstates

$$(A_1, A_2, G)^T = \mathcal{R}^P \mathcal{R}^G (a_d, a_u, a_s)^T, \tag{2.7}$$

which are ordered such that $M_{A_1} \leq M_{A_2}$.

At tree level the NMSSM Higgs sector can be parametrized by the six parameters

$$\lambda, \kappa, A_\lambda, A_\kappa, \tan\beta = \langle H_u^0 \rangle / \langle H_d^0 \rangle \quad \text{and} \quad \mu_{\rm eff} = \lambda \langle S \rangle. \tag{2.8}$$

The brackets around the fields denote the corresponding VEVs of the neutral components of the Higgs fields. The sign conventions for λ and $\tan\beta$ are chosen such that they are positive, while κ, A_λ, A_κ and $\mu_{\rm eff}$ can have both signs. Including the important higher order corrections, also the soft SUSY breaking mass terms for the scalars and the gauginos as well as the trilinear soft SUSY breaking couplings have to be taken into account.

III. THE NMSSM PARAMETER SCAN

We perform a scan in the NMSSM parameter space with the aim of finding scenarios that are compatible with the LHC Higgs search results and which lead to Higgs spectra that can be tested at the LHC with high c.m. energy, $\sqrt{s} = 13$ TeV. We demand them to contain at least one scalar Higgs boson with mass value around 125 GeV and rates that are compatible with those reported by the LHC experiments ATLAS and CMS.

We used the program package NMSSMTools [26,27] for the calculation of the SUSY particle and NMSSM Higgs boson spectrum and branching ratios. The higher order corrections to the NMSSM Higgs boson masses [16–20] have been incorporated in NMSSMTools up to $\mathcal{O}(\alpha_t \alpha_s + \alpha_b \alpha_s)$ for vanishing external momentum. The Higgs decays widths and branching ratios are obtained from NMHDECAY [26], an NMSSM extension of the Fortran code HDECAY [46,47]. The SUSY particle branching ratios are obtained from the Fortran code NMSDECAY [48] which is a generalisation of the Fortran code SDECAY [47,49] to the NMSSM particle spectrum. The NMSSM particle spectrum, mixing angles, decay widths and branching ratios are given out in the SUSY Les Houches Accord (SLHA) format [50]. For various parameter sets we have cross-checked the NMSSM Higgs branching ratios against the ones obtained with the recently released Fortran package NMSSMCALC [28]. Differences arise in the treatment of the radiative corrections to the Higgs boson masses and in the more sophisticated and up-to-date inclusion of the dominant higher order corrections to the decay widths as well as the consideration of off-shell effects in NMSSMCALC. The overall picture, however, remains unchanged.

We have performed the scan over a large fraction of the NMSSM parameter space in order to get a general view of the NMSSM Higgs boson phenomenology. For the mixing angle $\tan\beta$ and the NMSSM couplings λ and κ the following ranges have been considered,

$$1 \leq \tan\beta \leq 30, \qquad 0 \leq \lambda \leq 0.7, \qquad -0.7 \leq \kappa \leq 0.7. \tag{3.1}$$

We have taken care of not violating perturbativity by applying the rough constraint

$$\sqrt{\lambda^2 + \kappa^2} \leq 0.7. \tag{3.2}$$

The soft SUSY breaking trilinear NMSSM couplings A_λ and A_κ and the effective $\mu_{\rm eff}$ parameter have been varied in the ranges

$$-2 \text{ TeV} \leq A_\lambda \leq 2 \text{ TeV}, \qquad -2 \text{ TeV} \leq A_\kappa \leq 2 \text{ TeV},$$
$$-1 \text{ TeV} \leq \mu_{\rm eff} \leq 1 \text{ TeV}. \tag{3.3}$$

Note, that too large positive values for A_κ for negative κ lead to non-self-consistent solutions, which have been discarded. The parameter A_λ is related to the charged Higgs boson mass. The compatibility with the lower bound

on the charged Higgs mass has been checked for [51]. In the choice of the remaining soft SUSY breaking trilinear couplings and masses care has been taken to respect the exclusion limits on the SUSY particle masses [52–54]. The trilinear soft SUSY breaking couplings of the up- and down-type quarks and the charged leptons, A_U, A_D and A_L with $U \equiv u, c, t, D \equiv d, s, b$ and $L \equiv e, \mu, \tau$, are varied independently in the range

$$-2 \text{ TeV} \leq A_U, A_D, A_L \leq 2 \text{ TeV}. \tag{3.4}$$

The soft SUSY breaking right- and left-handed masses of the third generation are

$$\begin{aligned} 600 \text{ GeV} \leq M_{\tilde{t}_R} = M_{\tilde{Q}_3} \leq 3 \text{ TeV}, \\ 600 \text{ GeV} \leq M_{\tilde{\tau}_R} = M_{\tilde{L}_3} \leq 3 \text{ TeV}, \\ M_{\tilde{b}_R} = 3 \text{ TeV}. \end{aligned} \tag{3.5}$$

And for the first two generations we chose

$$M_{\tilde{u}_R, \tilde{c}_R} = M_{\tilde{d}_R, \tilde{s}_R} = M_{\tilde{Q}_{1,2}} = M_{\tilde{e}_R, \tilde{\mu}_R} = M_{\tilde{L}_{1,2}} = 3 \text{ TeV}. \tag{3.6}$$

The gaugino soft SUSY breaking masses finally are chosen to be positive and varied in the ranges

$$\begin{aligned} &100 \text{ GeV} \leq M_1 \leq 1 \text{ TeV}, \qquad 200 \text{ GeV} \leq M_2 \leq 1 \text{ TeV}, \\ &1.3 \text{ TeV} \leq M_3 \leq 3 \text{ TeV}. \end{aligned} \tag{3.7}$$

Negative gaugino masses M_1 and M_2 would affect the relic density, but change the features of the NMSSM Higgs sector only marginally. Note, that in NMSSMTOOLS the NMSSM-specific input parameters $\lambda, \kappa, A_\lambda$ and A_κ as well as all other soft SUSY breaking masses and trilinear couplings, according to the SLHA format, are understood as $\overline{\text{DR}}$ parameters taken at the SUSY scale $\tilde{M} = 1$ TeV, while $\tan\beta$ is taken at the mass of the Z boson, M_Z.

The program package NMSSMTOOLS is interfaced with MICROMEGAS [55] so that the compatibility of the relic abundance of the lightest neutralino as the NMSSM dark matter candidate with the latest PLANCK results [56] can be checked for. The package furthermore tests for the constraints from low-energy observables as well as from Tevatron and LEP. Details can be found on the webpage of the program [27].[2] In addition we have included in NMSSMTOOLS the latest LHC Higgs exclusion limits, given in Refs. [57–63]. Among the parameter points, that survive the constraints incorporated in NMSSMTOOLS, only those are kept that feature an NMSSM Higgs spectrum with at least one CP-even Higgs boson in the range of 124 to 127 GeV, which is fulfilled by either H_1 or H_2, and which will be denoted by h in the following. In some cases H_1 and H_2 are almost degenerate with a mass value near 125 GeV. In this case the signal rates observed at the LHC are built up by two Higgs bosons. Applying the narrow width approximation, the reduced signal rate μ_{XX} into a final state particle pair XX is given by the production cross section σ_{prod} of the NMSSM Higgs boson H_i times its branching ratio BR into the final state XX, normalized to the corresponding SM values for a SM Higgs boson H^{SM}, i.e.

$$\begin{aligned} \mu_{XX}(H_i) &= \frac{\sigma_{\text{prod}}(H_i) BR(H_i \to XX)}{\sigma_{\text{prod}}(H^{\text{SM}}) BR(H^{\text{SM}} \to XX)} \\ &\equiv R_{\sigma_{\text{prod}}}(H_i) R^{BR}_{XX}(H_i), \end{aligned} \tag{3.8}$$

with

$$M_{H^{\text{SM}}} = M_{H_i} \equiv M_h = 124\text{–}127 \text{ GeV}. \tag{3.9}$$

In Eq. (3.8) we have introduced the ratio of production cross sections

$$R_{\sigma_{\text{prod}}}(H_i) \equiv \frac{\sigma_{\text{prod}}(H_i)}{\sigma_{\text{prod}}(H^{\text{SM}})} \tag{3.10}$$

and the ratio of branching ratios

$$R^{BR}_{XX}(H_i) \equiv \frac{BR(H_i \to XX)}{BR(H^{\text{SM}} \to XX)}. \tag{3.11}$$

If not stated otherwise we approximate the inclusive cross section by the dominant gluon fusion production cross section. In the SM the loop induced process is mediated by top and bottom quark loops and known at next-to-leading order (NLO) QCD including the full mass dependence [64]. The next-to-next-to-leading order (NNLO) QCD corrections have been calculated in the heavy top mass approximation [65]. The latter is valid to better than 1% for Higgs masses below 300 GeV [66]. The soft gluon resummation [67,68] and partial, respectively approximate, next-to-next-to-next-to-leading order (N^3LO) results have been presented in [68,69]. In the NMSSM, gluon fusion production additionally contains stop and sbottom quark loops, with the squark loops becoming particularly important for squark masses below ~400 GeV [70]. The cross section can be adapted from the corresponding result in the MSSM [64,71], by replacing the respective MSSM Higgs-quark-quark and Higgs-squark-squark couplings with the NMSSM couplings. As we use in our scan the program package NMSSMTOOLS, which provides the ratio of the NMSSM Higgs boson decay width into a gluon pair at NLO QCD with respect to the NLO QCD decay width into gg of a SM Higgs boson with same mass, we approximate

[2]Note that in our analysis we do not take into account the constraint from $g-2$, as it is nontrivial to find parameter combinations which can explain the 2σ deviation from the SM value.

the gluon fusion production cross section for a CP-even NMSSM Higgs boson H_i by

$$\sigma^{\rm NMSSM}_{gg\to H_i} = \frac{\Gamma^{\rm NMSSM}_{\rm NLO}(H_i \to gg)}{\Gamma^{\rm SM}_{\rm NLO}(H^{\rm SM} \to gg)} \times \sigma^{\rm SM}_{gg\to H^{\rm SM}}, \quad \text{with} \quad M_{H_i} = M_{H^{\rm SM}}. \tag{3.12}$$

The SM gluon fusion cross section has been calculated at NNLO QCD for $M_{H^{\rm SM}} = 126$ GeV with the Fortran program HIGLU [72].[3] The cross section changes by less than 5% in the range 124 GeV $\lesssim M_{H^{\rm SM}} \lesssim$ 127 GeV. In NMSSMTools the gluon decay width does not include mass effects at NLO QCD. The higher order electroweak (EW) corrections [73] are of $\mathcal{O}(5\%)$ in the SM. As they are not available for the NMSSM and cannot be obtained by simple coupling modifications, we consistently neglect them.

TABLE I. The ATLAS and CMS combined signal rates and errors for the $bb, \tau\tau, \gamma\gamma, WW$ and ZZ final states. Apart from the bb final state, where Higgs-strahlung VH ($V = W, Z$) is the production channel, they are based on the inclusive production cross section. Details can be found in Refs. [74] and [75].

Channel	Best fit value	$2 \times 1\sigma$ error
$VH \to Vbb$	0.97	± 1.06
$H \to \tau\tau$	1.02	± 0.7
$H \to \gamma\gamma$	1.14	± 0.4
$H \to WW$	0.78	± 0.34
$H \to ZZ$	1.11	± 0.46

In case the signal is built up by the superposition of the rates from the 125 GeV h boson and another Higgs boson $\Phi = H_i, A_j$, which is almost degenerate, we define the reduced signal strength as

$$\mu_{XX}(h) \equiv R_{\sigma_{\rm prod}}(h) R^{BR}_{XX}(h) + \sum_{\substack{\Phi \neq h \\ |M_\Phi - M_h| \leq \delta}} R_{\sigma_{\rm prod}}(\Phi) R^{BR}_{XX}(\Phi) F(M_h, M_\Phi, d_{XX}). \tag{3.13}$$

Here δ denotes the mass resolution in the XX final state and $F(M_h, M_\Phi, d_{XX})$ the Gaussian weighting function as implemented in NMSSMTools. The experimental resolution d_{XX} of the channel XX influences the width of the weighting function. In the following only those parameter values are retained that lead to reduced rates according to Eq. (3.13) into the $bb, \tau\tau, \gamma\gamma, WW$ and ZZ final states, that are within 2 times the 1σ interval around the respective best fit value, as reported by ATLAS and CMS. Here we have combined the signal rates and errors, given in Refs. [74] and [75], of the two experiments according to Eq. (5) in [76]. The combined signal rates and errors are given in Table I.[4] Note, that in the following we will use the shorthand notation $2 \times 1\sigma$ to indicate the interval around the measured rate, that we allow for. In summary, in addition to the implemented restrictions in NMSSMTools, the conditions on our parameter scan are

$$\begin{aligned} &\text{At least one } CP\text{-even Higgs boson } H_i \equiv h \text{ with:} && 124 \text{ GeV} \lesssim M_h \lesssim 127 \text{ GeV} \\ &\text{Compatibility with } \mu^{\rm exp}_{XX}(X = b, \tau, \gamma, W, Z): && |\mu^{\rm scan}_{XX}(h) - \mu^{\rm exp}_{XX}| \leq 2 \times 1\sigma \end{aligned} \tag{3.14}$$

In our case we have $H_i = H_1$ or H_2, and $\mu^{\rm exp}_{XX}$ and $2 \times 1\sigma$ as given in Table I.

For all scenarios we require that they lead to relic densities $\Omega_c h^2$ that are not larger than the result given by PLANCK [56],

$$\Omega_c h^2 = 0.1187 \pm 0.0017. \tag{3.15}$$

While this can be achieved for a large fraction of parameter points, there are only a few points that reproduce the relic density within the given errors. This is to be expected, however, in view of the remarkably small error on the relic density reported by PLANCK.

IV. RESULTS

In this section we first present the general features of the scenarios as the outcome of our scan that survive all imposed constraints. Subsequently the parameter sets shall be investigated in more detail with respect to their prospects of discovering NMSSM Higgs bosons or testing the coupling structure of the Higgs sector.

A. NMSSM and stop sector parameter distributions

Figure 1 (left) shows the distribution of the λ and κ values for the scenarios resulting from our scan. The right figure shows the viable values in the $\tan\beta - \lambda$ plane. The

[3] For comparison we also calculated for some parameter points the NMSSM Higgs production cross sections at NNLO with HIGLU. For the SM-like Higgs boson the approximation Eq. (3.12) works better than 1%. For the heavy MSSM-like Higgs bosons there can be deviations of up to $\mathcal{O}(10\%)$, and for the light singletlike Higgs bosons they can reach the level of $\mathcal{O}(20\%)$ for some scenarios. For our purposes the approximation is good enough.

[4] In order to check the compatibility in the $b\bar{b}$ final state we have replaced gluon fusion production with production in association with W, Z.

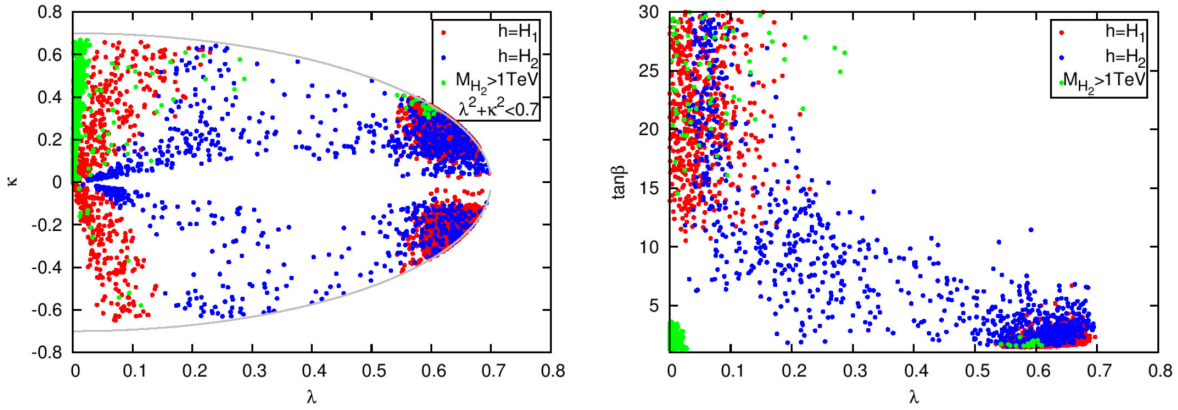

FIG. 1 (color online). Parameter distributions in the $\kappa - \lambda$ plane (left) and in the $\tan\beta - \lambda$ plane (right). The SM-like Higgs boson h corresponds to either H_1 (red points) or H_2 (blue points). Green points correspond to $h \equiv H_1$ and H_2 mass values above 1 TeV.

particular shape of the $\kappa - \lambda$ distribution is the result of the requirement Eq. (3.2). As can be inferred from the figures, in the scenarios passing the constraints either the lightest Higgs boson H_1 (red points) or the second lightest H_2 (blue points) is the SM-like Higgs boson h with mass around 125 GeV. While the λ and κ values cover the whole allowed region, most scenarios are found for either low ($\lesssim$0.1) or high ($\gtrsim$0.55) λ values. In the low-λ region in particular κ values close to 0 lead to the H_2 being the SM-like Higgs boson, higher κ values imply the lightest scalar boson to have SM properties. For small λ values and κ nonzero the singletlike Higgs boson is at tree-level already comparatively heavy, so that it corresponds to the second lightest Higgs boson and H_1 is SM-like. If, however, κ is also small the singlet mass becomes smaller than 125 GeV so that H_2 can be SM-like. Large λ values allow independently of κ for either H_1 or H_2 being SM-like. Note, however, that in this region, κ values close to zero are precluded.[5]

Figure 1 (right) shows the well known fact that in the NMSSM large λ values (∼0.5–0.7) in conjunction with small $\tan\beta$ values below ∼5 allow for the lightest or next-to-lightest scalar Higgs to be SM-like around 125 GeV. The other parameter combination leading to scenarios compatible with the Higgs data, though less in number, is the combination of $\lambda \lesssim 0.1$ and $\tan\beta \gtrsim 10$. This is in accordance with the behavior of the upper mass bound on the MSSM-like light Higgs boson given by

$$m_h^2 \approx M_Z^2 \cos^2 2\beta + \frac{\lambda^2 v^2}{2} \sin^2 2\beta + \Delta m_h^2, \qquad (4.1)$$

with $v \approx 246$ GeV, and which is to be identified with the SM-like Higgs h at 125 GeV after the inclusion of the radiative corrections Δm_h^2. Also for intermediate λ values viable scenarios can be found, although, being away from the maximum of the function Eq. (4.1), only for $h \equiv H_2$. For the lightest CP-even Higgs in this case the tree-level mass bound is too low to be shifted through radiative corrections to large enough mass values compatible with all constraints imposed.

Note that in scenarios, where $M_{H_1} < 125$ GeV, this Higgs boson is mostly singletlike thus escaping the constraints from LEP, Tevatron and LHC searches in this mass region. The strategies to search for H_1 in this case shall be discussed in the next section. We also found scenarios where the mass of the second lightest scalar H_2 is larger than 1 TeV and can indeed become very large. This large increase is caused by either small λ values or large values for A_λ or $\mu_{\rm eff}$. As these scenarios are extremely fine-tuned we will discard them in the following investigations from Fig. 5 on.

Figure 2 shows the $\tan\beta$ and $\mu_{\rm eff}$ distributions. Note that for the $\tan\beta$ distribution we use a logarithmic scale. Most $\tan\beta$ values are clustered around $\tan\beta \approx 2$. The range of the effective $\mu_{\rm eff}$ values is 100 GeV $\lesssim |\mu_{\rm eff}| \lesssim 1$ TeV. Absolute $\mu_{\rm eff}$ values of less than ∼100 GeV are excluded due to the lower bounds on the chargino masses.

The distributions of the NMSSM parameters λ, κ, A_λ and A_κ normalized to the total number of parameter points of about 8000 are shown in Fig. 3. The λ values cluster close to 0 and around 0.65, the preferred κ values are close to −0.25 and +0.25. The preferred values of A_κ around 0 can be understood by the fact that this is the range of A_κ allowing for the lightest scalar and pseudoscalar masses

[5]In the limit when κ goes to zero the mass of the lightest neutralino $m_{\tilde{\chi}_1^0}$, which is predominantly singlino, becomes much smaller than M_Z and the couplings of this state to the SM particles and their superpartners tend to be negligibly small leading to rather small annihilation cross section for $\tilde{\chi}_1^0\tilde{\chi}_1^0 \to$ SM particles. Since the dark matter density is inversely proportional to the annihilation cross section at the freeze-out temperature such a light neutralino state gives rise to a relic density that is typically substantially larger than its measured value. As a result κ values close to zero are basically ruled out, unless there also exists a very light CP-even or CP-odd Higgs state with mass $\approx 2m_{\tilde{\chi}_1^0}$ that can facilitate lightest neutralino annihilation (for a recent discussion see [43]).

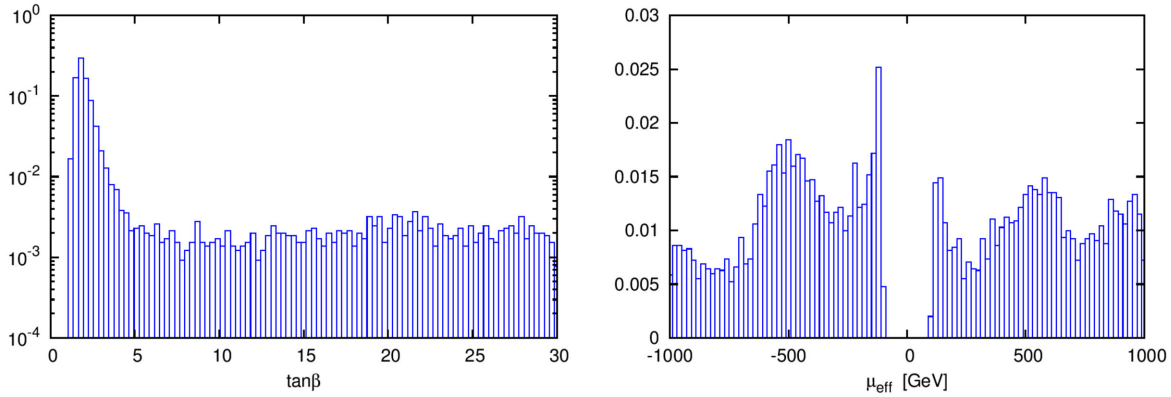

FIG. 2 (color online). Distribution of $\tan\beta$ (left) and $\mu_{\rm eff}$ (right). Normalized to the total number of parameter points of ∼8000.

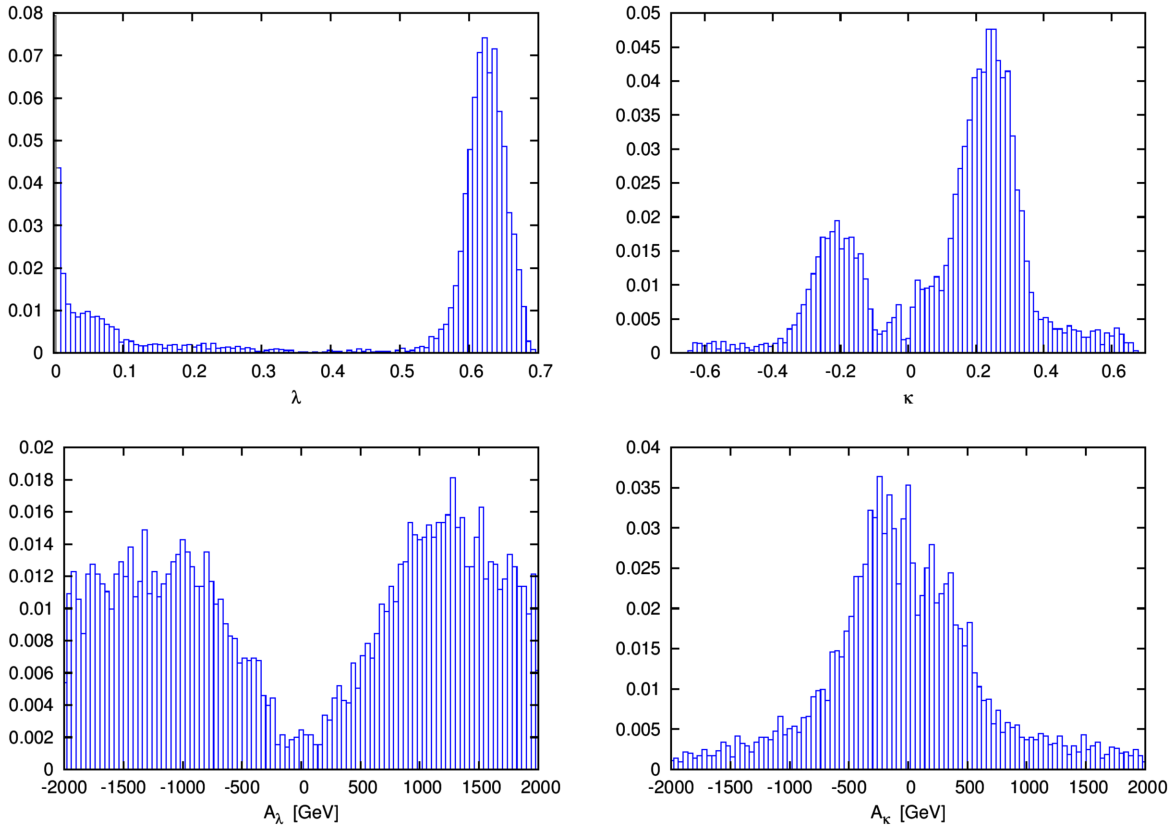

FIG. 3 (color online). Upper: Distribution of λ (left) and κ values (right). Lower: Distribution of A_λ (left) and A_κ values (right). Normalized to the total number of parameter points of ∼8000.

squared to be positive.[6] For A_λ larger values are preferred, as these lead to sufficiently heavy Higgs bosons [77], that are not excluded by the experiment and entail a heavy enough SM-like Higgs boson. All these considerations of course apply modulo the higher order corrections which are indispensable to shift the SM-like Higgs boson mass to 125 GeV. These corrections are dominated by the (s)top loop contributions.

[6]This range has been derived in [77] applying approximate tree-level mass formulas.

The distributions of the trilinear soft SUSY breaking stop-sector coupling A_t and of the lightest stop mass $m_{\tilde{t}_1}$ are shown in Fig. 4. Due to the additional contribution proportional to λ to the tree-level mass, cf. Eq. (4.1), less important radiative corrections Δm_h^2 are necessary to shift m_h to 125 GeV. Contrary to the MSSM, therefore zero mixing in the stop sector leads to allowed scenarios in the NMSSM. For the same reason, the lightest stop mass can still be rather light, down to about 270 GeV. The upper bound is limited by our scan range. Experiments set a low mass bound in searches for stop quarks decaying into a

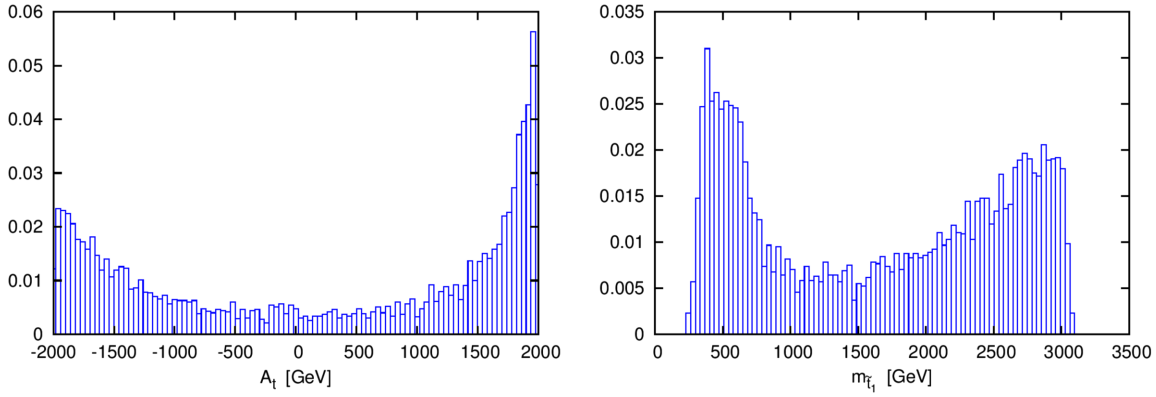

FIG. 4 (color online). Distribution of A_t (left) and $m_{\tilde{t}_1}$ (right), normalized to the total number of parameter points of ~8000.

charm quark and the lightest neutralino, $\tilde{\chi}_1^0$ [53,78–81].[7] This is the dominating decay for mass differences $m_{\tilde{t}_1} - m_{\tilde{\chi}_1^0} < M_W$, where M_W denotes the charged W boson mass, [85,86]. The latest results by ATLAS [53] exclude top squark masses up to about 240 GeV at 95% C.L. for arbitrary neutralino masses, within the kinematic boundaries.

The distribution for A_t peaks at large values of $\sim \pm 2$ TeV. Large A_t values entail large radiative corrections to the SM-like Higgs boson mass, so that the tree-level mass value can be shifted to the required 125 GeV. At the same time this results in a large splitting of the stop mass values, so that the lightest stop mass $m_{\tilde{t}_1}$ distribution reaches its maximum around 500 GeV. Another accumulation is at the upper $m_{\tilde{t}_1}$ range as a result of large radiative mass corrections induced by heavy stop masses.

B. Mass distributions

In Fig. 5 we show the mass distribution for the non-SM-like H_i, which is either H_1 or H_2, versus the lightest pseudoscalar mass values M_{A_1}. For mass values below about 115 GeV the non-SM-like Higgs boson is H_1, while for $M_{H_i} \gtrsim 170$ GeV it is H_2. There is a gap for 115 GeV $\lesssim M_{H_i} \lesssim 170$ GeV and another one for 115 GeV $\lesssim M_{A_1} \lesssim$ 130 GeV. Both are due to the LHC exclusion limits. There are only a few points for $M_{H_i}, M_{A_1} \lesssim 62$ GeV. Here the decay of the SM-like 125 GeV Higgs boson into very light scalars or pseudoscalars would be kinematically possible, inducing reduced branching ratios in the SM decays and hence reduced signal rates not compatible with the experiment any more. The blue (pink) points denote scenarios with $\tan\beta < (>)5$. Both low and high $\tan\beta$ values yield scenarios with $H_2 \equiv h$ (here $M_{H_i} \equiv M_{H_1} \lesssim 115$ GeV). Scenarios with the lightest scalar being SM-like arise mostly for low $\tan\beta$ values, since then the tree-level mass of the lightest MSSM-like Higgs boson is maximized. As

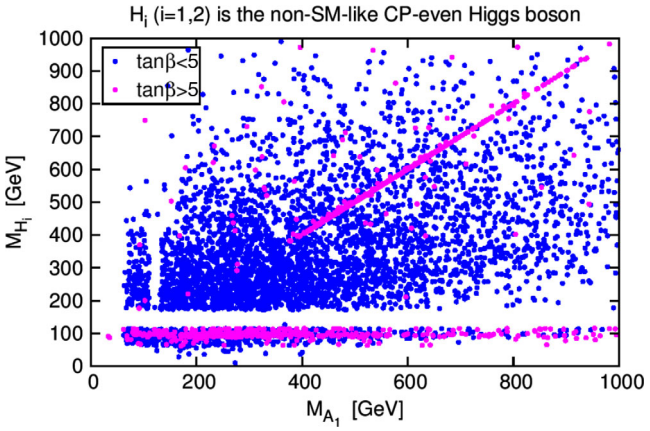

FIG. 5 (color online). Mass values of the non-SM-like CP-even Higgs boson H_i ($i = 1$ or 2) and the lightest pseudoscalar A_1 for all points passing our constraints. Blue (pink) points are for scenarios with $\tan\beta < (>)5$.

can be inferred from the plot, for large $\tan\beta$ values and mass values above ~400 GeV, the mass values of $H_i(\equiv H_2)$ are (almost) equal to those of A_1. Here, both H_i and A_1 are MSSM-like with almost the same mass [77]. Figures 6 show the amount of singlet component of H_i, $|S_{H_i,h_s}|^2$ (upper left), and A_1, $|P_{A_1,a_s}|^2$ (upper right), as a function of M_{H_i} and M_{A_1}, respectively.[8] Values of 1 (0) correspond to pure singletlike (MSSM-like) states. For mass values above 400 GeV and $\tan\beta > 5$, H_i and A_1 can be MSSM-like.

In general the mass values of H_1 are 35 GeV$\lesssim M_{H_1} \lesssim 115$ GeV, the lowest possible mass values for A_1 are $M_{A_1} \gtrsim 30$ GeV, ranging up to $\mathcal{O}$(TeV), and for the next-to-lightest scalar we have 170 GeV$\lesssim M_{H_2} \lesssim \mathcal{O}$(TeV). The masses of the heavier Higgs bosons H_3 and A_2 lie between about 300 GeV up to $\mathcal{O}$(TeV). Their singlet

[7]Investigating the stop four-body decays into a neutralino, bottom quark and fermion pair [82,83], similar bounds can be derived in the searches for monojets [53,84].

[8]The matrix S corresponds to the rotation matrix $\mathcal{R}^S$ Eq. (2.6), however taking into account loop corrections to the scalar Higgs mass eigenstates. Accordingly P corresponds to the matrix $(\mathcal{R}^P\mathcal{R}^G)$ Eq. (2.7), performing the rotation from the interaction to the loop corrected pseudoscalar mass eigenstates.

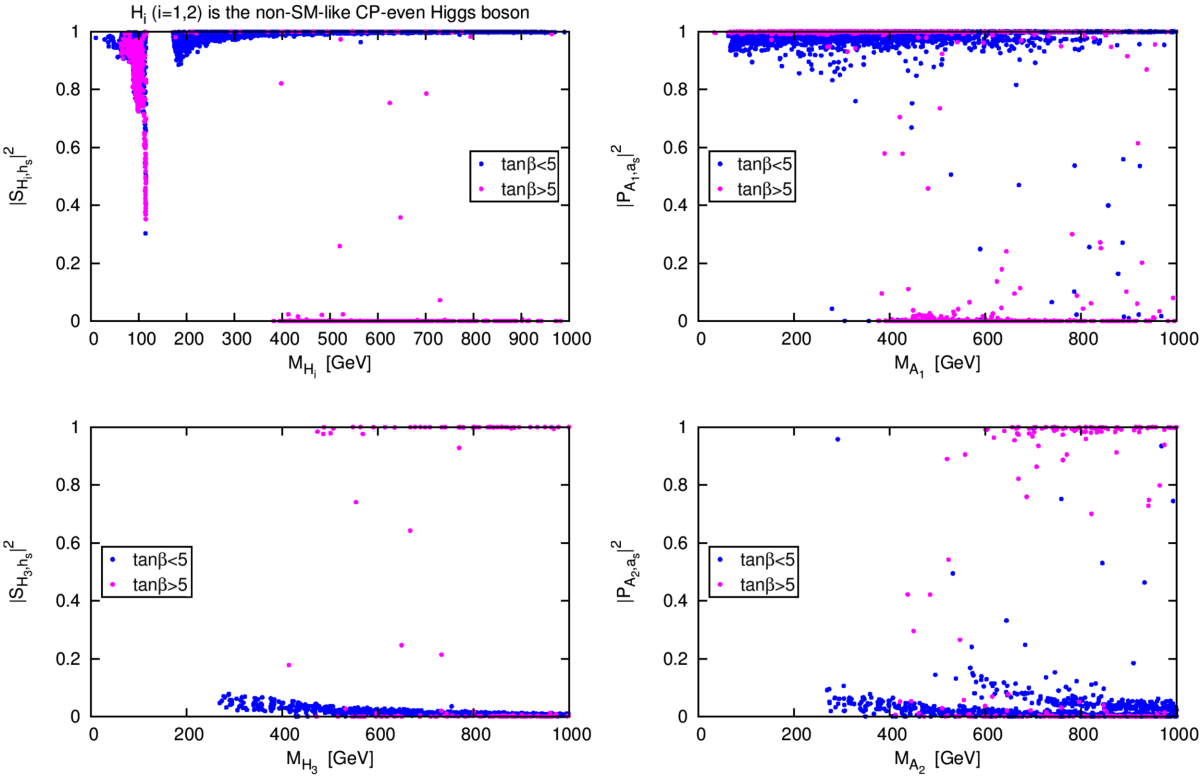

FIG. 6 (color online). The singlet component $|S_{H_i,h_s}|^2$ of the non-SM-like CP-even Higgs boson H_i (upper left), $|P_{A_1,a_s}|^2$ of the lightest pseudoscalar A_1 (upper right), $|S_{H_3,h_s}|^2$ of the heavy CP-even Higgs boson H_3 (lower left) and $|P_{A_2,a_s}|^2$ of the heavy pseudoscalar A_2 (lower right). Blue (pink) points refer to scenarios with $\tan\beta < (>)5$.

components $|S_{H_3,h_s}|^2$ and $|P_{A_2a_s}|^2$ are shown in Fig. 6 (lower left) and (lower right), respectively.

The singlet-/doublet-composition of the various Higgs bosons determines their production and decay rates, which depend on the Higgs coupling strengths to the SM-particles, and hence their discovery prospects. Inspection of the singlet components for the two $\tan\beta$ ranges below and above 5 and the scenarios with either H_1 or H_2 being SM-like reveals the approximate pattern for the compositions of the NMSSM Higgs bosons, given in Table II. Note that for an SM-like H_2 the lightest $H_{i=1}$ can become doubletlike in the regions with strong singlet-doublet mixing, i.e. in mass regions close to 125 GeV. The unitarity of the mixing matrix does not allow for all Higgs bosons being simultaneously doubletlike, so that alternative search techniques for the Higgs bosons with significant singlet component, like Higgs-to-Higgs decays or SUSY particle decays into Higgs bosons, have to be exploited. Another class of scenarios are those with Higgs bosons that mix strongly and that are not exclusively singlet- or doubletlike. They may challenge the Higgs searches by too small cross sections and/or Higgs signals built up by more than one Higgs boson.[9]

C. Signal rates

In order to investigate the discovery prospects of the non-SM-like NMSSM Higgs bosons, we analyze in the following their signal rates in various SM particle final states.

Signal rates for the non-SM-like H_i ($i = 1, 2$): Figure 7 shows the production rates in pb at a c.m. energy of $\sqrt{s} = 13$ TeV for the non-SM-like CP-even Higgs boson H_i ($i = 1, 2$) in the $\gamma\gamma$, $b\bar{b}$, ZZ and $t\bar{t}$ final states. The inclusive production cross section has been approximated by the dominant gluon fusion production mechanism. The production rates of H_i, $\sigma_{XX}(H_i)$, have been calculated in the narrow width approximation by multiplying the production cross section in gluon fusion at 13 TeV[10] with the branching ratios into the various SM particle final states,

$$\sigma_{XX}(H_i) \equiv \sigma^{13\ \mathrm{TeV}}_{ggH_i} BR_{H_i\to XX}, \qquad X = \gamma, b, \tau, W^{\pm}, Z, t. \tag{4.2}$$

The NMSSM gluon fusion production cross section has been obtained according to Eq. (3.12), and the branching ratios have been taken from NMSSMTools in order to be consistent with the NMSSM mass values, which we have

[9]The resolution of degenerate Higgs signals will require particularly high luminosity accumulated at the end of the LHC operation [15,87], and this discussion is not subject of this paper.

[10]Gluon fusion production increases by ∼12% for a Higgs mass of 90 GeV up to ∼19% for a Higgs mass of 300 GeV when increasing the c.m. energy from 13 to 14 TeV.

TABLE II. The approximate singlet-/doublet-composition of the NMSSM Higgs bosons for small and large $\tan\beta$ values and scenarios with either H_1 (left) or H_2 (right) SM-like.

$\tan\beta < 5$	$H_{i=1}$ SM-like	$H_{i=2}$ SM-like
$H_{j=1,2\neq i}$	singlet	singlet- up to almost doublet
H_3	doublet	doublet
A_1	mostly singlet (few doublet)	mostly singlet (few doublet)
A_2	mostly doublet (few singlet)	mostly doublet (few singlet)
$\tan\beta \geq 5$	$H_{i=1}$ SM-like	$H_{i=2}$ SM-like
$H_{j=1,2\neq i}$	mostly doublet	singlet- up to almost doublet
H_3	singlet (few doublet)	doublet
A_1	doublet or singlet (for small M_{A_1})	doublet or singlet (for small M_{A_1})
A_2	singlet or doublet	singlet or doublet

obtained at 2-loop order from NMSSMTOOLS. The black line corresponds to the SM Higgs boson production rate with the same mass as H_i. Again the points with mass values below ~115 GeV correspond to $H_i = H_1$ and hence H_2 being SM-like, while for mass values $\gtrsim$170 GeV we have H_1 taking the SM role and $H_i = H_2$. For large values of $\tan\beta$, the dominant production channel is associated production of the Higgs bosons with a $b\bar{b}$ pair. We have computed these cross sections by multiplying the SM cross section, computed at NNLO with the code SUSHI [88] at the same mass value as the NMSSM Higgs boson, with the NMSSM Higgs coupling squared to the b-quark pair in terms of the SM coupling. With the exception of small mass values, for large $\tan\beta$ values the cross sections are roughly a factor 10 larger than the gluon fusion result. If not stated otherwise, we do not show separate plots for this case, but assume implicitly that for $\tan\beta > 5$ larger rates are possible through associated production, thus ameliorating the discovery prospects.

(a) Signal rates for $H_{i=1}$: For small Higgs masses H_1 is singletlike, but can be more doubletlike in the mass regions close to 125 GeV. The photonic final state rate can then

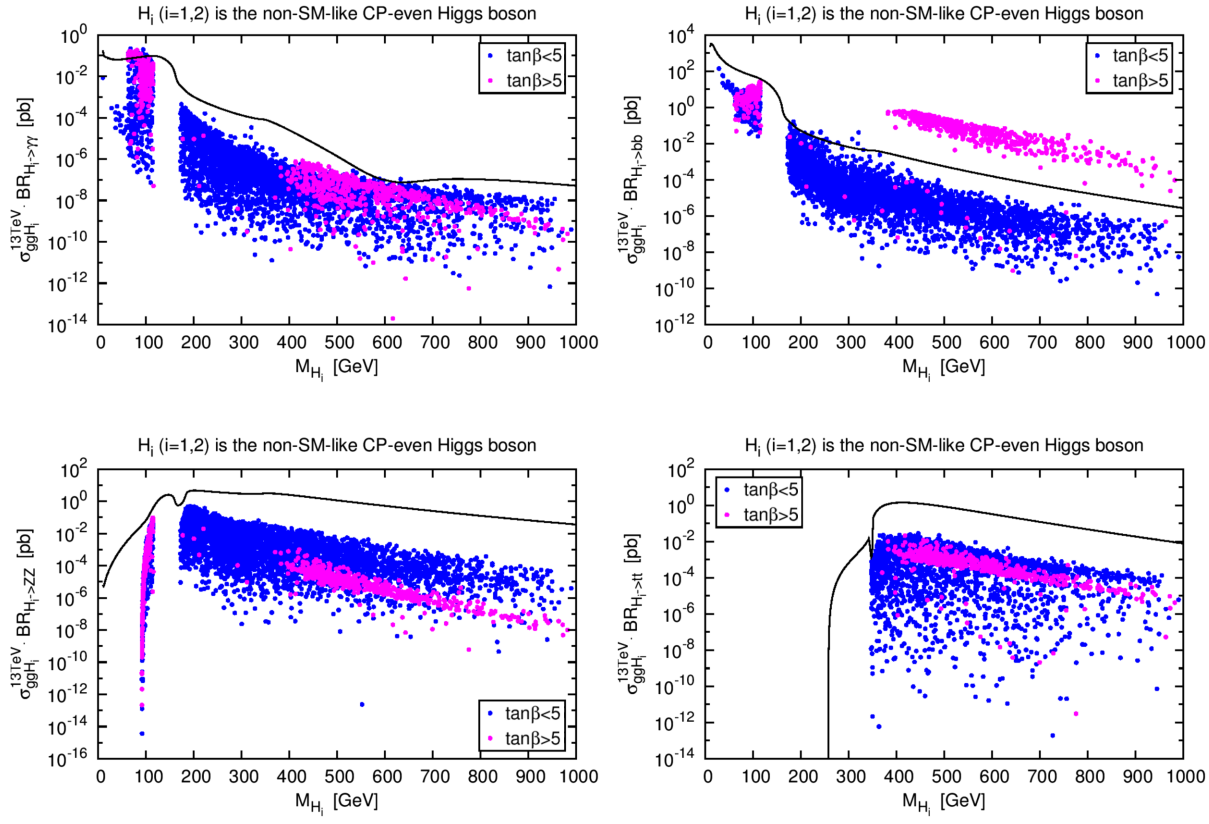

FIG. 7 (color online). Production rates in pb for the non-SM-like CP-even Higgs boson H_i ($i = 1, 2$) into the $\gamma\gamma$ (upper left), the $b\bar{b}$ (upper right), the ZZ (lower left) and $t\bar{t}$ (lower right) final states for $\tan\beta < 5$ (blue) and $\tan\beta > 5$ (pink), as a function of M_{H_i} at a c.m. energy $\sqrt{s} = 13$ TeV. The full black line shows the production rate for a SM Higgs boson with same mass.

even exceed the corresponding SM result, cf. Fig. 7 (upper left). For the photonic final state in inclusive SM Higgs boson production at leading order, ATLAS studies [89] have been performed for Higgs masses between 80 and 150 GeV at $\sqrt{s} = 14$ TeV and 100 fb^{-1} integrated luminosity. From these it may be concluded, that taking into account higher order corrections to the production cross section [90], which increase the cross section by about a factor 2, a SM Higgs boson could be discovered down to about 80 GeV if both ATLAS and CMS accumulate 300 fb^{-1} each. A light scalar NMSSM Higgs boson may hence be discovered in the photonic final state for scenarios where its rates are of the order of the SM ones.

Further possible discovery modes might be the $b\bar{b}$ and/or $\tau\tau$ final states in the regions, where the rates are compatible with the ones of a SM Higgs boson, i.e. for M_{H_i} close to 115 GeV. The $\tau\tau$ final states are not shown in Fig. 7, but exhibit the same pattern as the $b\bar{b}$ final state with an additional suppression factor of 10. The Z and $W^{\pm}$ boson final states reach maximum signal rates of about 0.1 pb for the former and 1 pb for the latter. Again the $W^{\pm}$ final states, not depicted in Fig. 7, show the same behavior as the Z boson final states. They are enhanced by a factor 10 compared to these, however with missing energy in the final state, so that only transverse Higgs masses can be reconstructed.

(b) Signal rates for $H_{i=2}$: We now turn to possible discovery channels for H_2 being the non-SM-like Higgs boson, hence investigate the mass regions above 170 GeV in Fig. 7. The next-to-lightest Higgs boson H_2 with $H_1 \equiv h$ is mostly singletlike for small $\tan\beta$ values and mostly doubletlike for $\tan\beta \geq 5$. The SM-like Higgs H_1 needs to be doubletlike with a large H_u component, in order to have a substantial coupling to top quarks and hence a gluon fusion cross section large enough to lead to signal rates compatible with the LHC data. Due to the unitarity of the mixing matrix $\mathcal{R}^S$ rotating the current to the mass eigenstates, H_2 is hence doubletlike but with a large H_d component, so that its couplings to down-type fermions are enhanced compared to the SM. The coupling G_{H_iVV} to massive vector bosons $V = Z, W^{\pm}$ on the other hand is suppressed. This can be understood by looking at the coupling, which normalized to the SM coupling is given by

$$\frac{G_{H_iVV}}{g_{H^{\rm SM}VV}} \equiv g_{H_iVV} = (\mathcal{R}^S_{i1}\cos\beta + \mathcal{R}^S_{i2}\sin\beta), \quad (4.3)$$

where $\mathcal{R}^S_{i1}$ ($\mathcal{R}^S_{i2}$) quantifies the H_d (H_u) component of H_i. The H_d component can be substantial for large $\tan\beta$ but its contribution in the coupling is suppressed by the factor $\cos\beta$. The up-type part of the coupling comes with $\sin\beta$ and also for small $\tan\beta$ values would be small, as the H_u component is taken by $H_1 \equiv h$. As can be inferred from the plot, for Higgs mass values above ~400 GeV the rates into $b\bar{b}$ are enhanced for large $\tan\beta$. This is due to an enhanced branching ratio into bottom pairs. The total decay width in this mass range is dominated by the decay into $V = W, Z$, and the H_2 branching ratio into $b\bar{b}$ can be approximated by

$$\begin{aligned}\mathrm{BR}^{\rm NMSSM}_{H_2\to b\bar{b}} &= \frac{g^2_{H_2d\bar{d}}\Gamma^{\rm SM}_{H^{\rm SM}\to b\bar{b}}}{g^2_{H_2VV}\Gamma^{\rm SM}_{H^{\rm SM}\to WW} + g^2_{H_2VV}\Gamma^{\rm SM}_{H^{\rm SM}\to ZZ} + \cdots} \\ &\approx \frac{g^2_{H_2d\bar{d}}}{g^2_{H_2VV}}\mathrm{BR}^{\rm SM}_{H^{\rm SM}\to b\bar{b}}, \end{aligned} \quad (4.4)$$

with $M_{H_2} = M_{H^{\rm SM}}$ and where $g_{H_2d\bar{d}}$ denotes the H_2 coupling to down-type fermions in terms of the SM coupling. The enhanced coupling to down-type quarks and the suppressed coupling to massive gauge bosons explain the observed behavior.

For large values of $\tan\beta$ and mass values above 400 GeV, the heavier H_2 may therefore be discovered in its $b\bar{b}$ and $\tau\tau$ final state, which exhibits the same behavior as the $b\bar{b}$ final state, the latter suffering from large backgrounds though, so that the τ production rate, suppressed by roughly a factor 10 compared to the former, may be more promising for discovery. In particular, the production in association with a b-quark pair (not shown here) increases the signal rates by another factor ~10 compared to production in gluon fusion. The gauge boson and top quark final states are more challenging on the other hand, even in associated production, due to the (above discussed) suppression of the couplings to gauge bosons and top quarks. For $\tan\beta \lesssim 5$ the H_2 searches have to rely on a combined search in the $\tau\tau$ final states (most interesting for H_2 masses up to ~250 GeV) and the vector-boson and top-pair channels. The associated production with b-quarks is not effective for these $\tan\beta$ values.

Production rates of A_1: Figure 8 displays the signal rates for the lightest CP-odd Higgs boson A_1 produced in association with a b-quark pair in the $b\bar{b}$ final state (left) and in gluon fusion in the top quark decay (right). The rates into $\tau\tau$ and $\mu\mu$ final states show the same pattern as the ones into $b\bar{b}$ but are suppressed by a factor of 10 and ~10^4 each. Massive gauge boson final states are forbidden due to the CP-odd nature of A_1. The decay rates into photons both in associated and in inclusive production are below 10^{-4} already in the low-mass range. In this mass range A_1 may be discovered in its decays into τ's, as the b-quark final states are notoriously difficult due to large backgrounds. This discovery channel is also interesting for large M_{A_1} at $\tan\beta > 5$. For $M_{A_1} \gtrsim 400$ GeV the pseudoscalar, which in most scenarios is singletlike, can also be MSSM-like with a large a_d component, in particular for $\tan\beta > 5$, cf. Fig. 6. Associated production with a b-quark pair here leads to cross sections of up to 4 pb. Otherwise the top quark final state has to be exploited for heavy A_1 production, though challenging with cross sections of at most a few pb and a complicated final state. We note, that for small $\tan\beta$ values, there is a step in Fig. 8 in the areas covered by the scatter

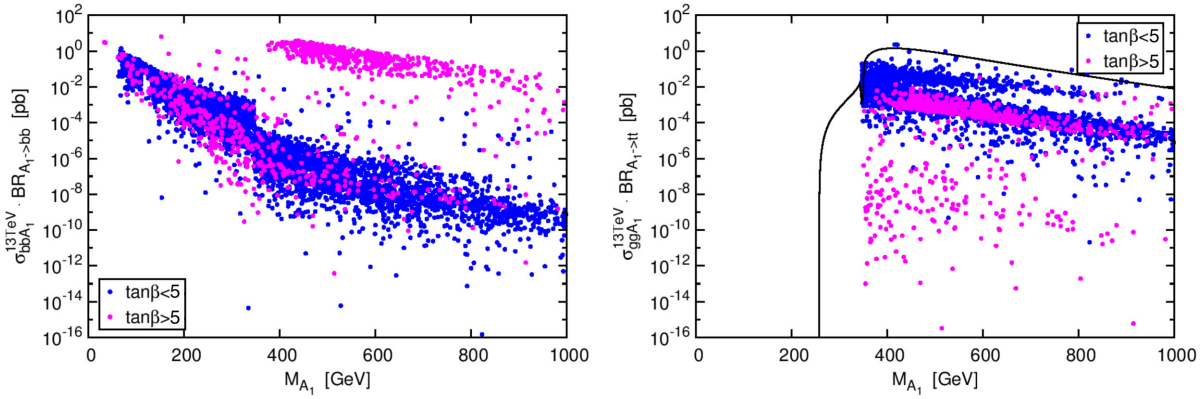

FIG. 8 (color online). Production rates in pb for the lightest CP-odd Higgs boson A_1 in associated production with $b\bar{b}$ in the $b\bar{b}$ final state (left) and in inclusive production with subsequent decay into $t\bar{t}$ final states (right) $\tan\beta < 5$ (blue) and $\tan\beta > 5$ (pink), as a function of M_{A_1}, at $\sqrt{s} = 13$ TeV. The full black line is the production rate for a SM Higgs boson with same mass.

points around $M_{A_1} = 350$ GeV. This is due to the opening of the decays into the top pair final state, which steeply increase at the top pair threshold and therefore cause a rapid fall in the branching ratios into the other final states. For large $\tan\beta$ the decay into top quarks does not play a role, so that there is no such behavior for the scatter points at large $\tan\beta$ values.

Heavy H_3 production: Apart from large $\tan\beta$ values with a SM-like H_1 boson, the H_3 is mostly doubletlike, however with a large H_d component so that the couplings to gauge bosons are suppressed, as discussed previously, likewise the couplings to top quarks. The branching ratios into bottom and top quark pairs, however, can be enhanced due to the small coupling to gauge bosons, as the total width in this heavy mass region is dominated by the decays into the latter. Figure 9 (upper) shows the production rates for the heaviest CP-even, H_3, into the $b\bar{b}$ and the $t\bar{t}$ final states. In the $b\bar{b}$ final state the rates are at most 0.5 pb in the lower mass region, where the SM-like Higgs boson is mostly H_1 and below 0.01 pb above about 400 GeV, where the SM-like resonance can also be H_2. In τ pair final states they are a factor 10 lower. For large $\tan\beta$ values the rates can be enhanced by about roughly a factor 10 in $b\bar{b}H_3$ production. In the top quark pair final states the cross sections are somewhat larger ranging from ~5 pb at the threshold to $\mathcal{O}(0.01)$ pb for $\tan\beta < 5$. For large $\tan\beta$ the $t\bar{t}$ production rates are below 0.05 pb. The rates into WW range for $\tan\beta < 5$ maximally between 1 pb and 10^{-4} pb in 250 GeV $\lesssim M_{H_3} \lesssim 1$ TeV, cf. Fig. 9 (lower left). For the ZZ final state they are somewhat smaller. For large $\tan\beta$ values these final states are not interesting. The photonic final state rates, finally, are below 10^{-4} pb.

Heavy A_2 production: The heavy pseudoscalar A_2 production rates in the $b\bar{b}$ and $t\bar{t}$ final states, as well as the photonic mode show almost the same pattern as the ones for H_3 with the same absolute values, and the same conclusions as for the H_3 searches apply. The pseudoscalar cannot decay into gauge bosons, so that these final states cannot be exploited here.

The above results show that the discovery of *all* NMSSM Higgs bosons is not straightforward and additional alternative discovery modes need to be exploited, which shall be discussed in the following sections. Before doing so, let us briefly review what the current experimental status is. So far, dedicated searches in the NMSSM have been performed by CMS for a very light pseudoscalar with mass between 5.5 and 14 GeV, decaying into a μ pair, for which exclusion limits have been derived [91]. The ATLAS experiment has investigated the decay chain for a heavy CP-even Higgs boson into a light pseudoscalar Higgs pair, that subsequently decays into photons, $H \to aa \to \gamma\gamma + \gamma\gamma$ [92]. The signal has been studied using simulated samples over a range of Higgs boson masses between 110 and 150 GeV and for three a boson masses, $M_a = 100, 200$ and 400 MeV. For a c.m. energy of 7 TeV and 4.9 fb^{-1} integrated luminosity, the derived 95% confidence level (C.L.) exclusion limits on the cross section times branching ratio are 0.1 pb in the Higgs boson mass range between 115 and 140 GeV and ~0.2 pb in the region outside. Recently CMS has published results on the search for the resonant production of Higgs pairs in the decay channel $X \to HH \to \gamma\gamma + b\bar{b}$ using 19.7 fb^{-1} integrated luminosity collected at $\sqrt{s} = 8$ TeV [93]. For the investigated mass range between $m_X = 260$ and 1100 GeV upper limits at 95% C.L. on the cross section have been extracted between about 4 and 0.4 fb. The ATLAS experiment has performed searches for resonant and nonresonant Higgs boson pair production in the $hh \to \gamma\gamma b\bar{b}$ final state at a c.m. energy of 8 TeV and an integrated luminosity of 20.3 fb^{-1} [94]. Assuming SM branching ratios a 95% C.L. upper limit of 2.2 pb is extracted on the cross section times branching ratio of the nonresonant production. The corresponding limit observed for a narrow resonance lies between 0.8 and 3.5 pb depending on its mass. Extrapolating these results to the high-energy LHC with up to 300 fb^{-1} integrated

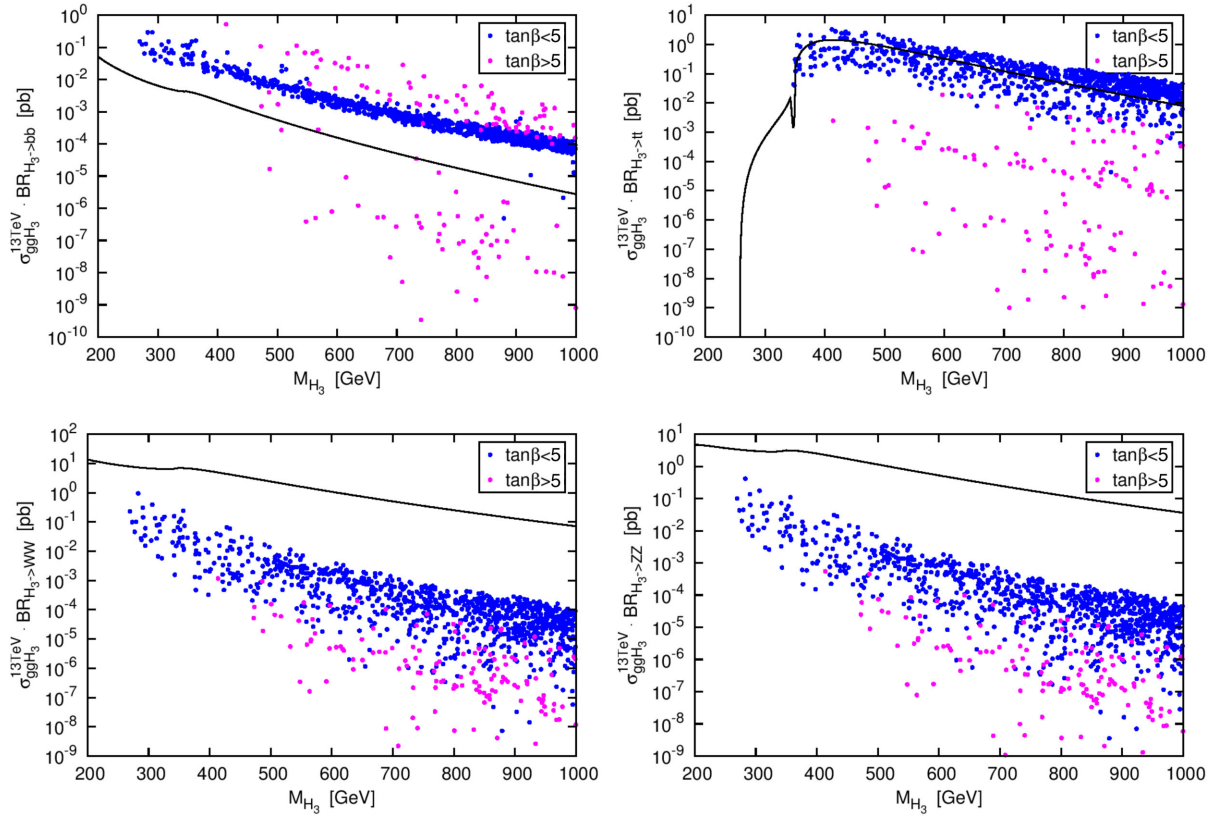

FIG. 9 (color online). Production rates in pb for the heaviest CP-even Higgs boson H_3 into the $b\bar{b}$ (upper left), the $t\bar{t}$ (upper right), the WW (lower left) and ZZ (lower right) final states for $\tan\beta < 5$ (blue) and $\tan\beta > 5$ (pink), as a function of M_{H_3}, at $\sqrt{s} = 13$ TeV. The full black line is the production rate for a SM Higgs boson with same mass.

luminosity per experiment, decay cross sections for Higgs-to-Higgs decays with subsequent Higgs decays into the $(\gamma\gamma)(b\bar{b})$ final states down to $\mathcal{O}(\text{fb})$ should be large enough for detection.

V. DISCOVERING NATURAL NMSSM AT THE LHC

In the previous section we have discussed the signal rates that can be expected in the NMSSM parameter space that is left over after applying all constraints set by the Higgs search results from experiment and by the relic density. In this section now we investigate that subspace of the NMSSM, that we found to give the best discovery prospects at the high-energy LHC for all of the neutral NMSSM Higgs bosons and that can hence strongly be constrained at the next run of the LHC. Such part of the NMSSM parameter space is given by what we call the natural NMSSM. It is characterized by an approximate Peccei-Quinn symmetry,[11] hence small κ values, by rather small $|\mu_{\text{eff}}|$ values and by small $\tan\beta$. In particular we choose the following part of the NMSSM parameter space

$$0.6 \le \lambda \le 0.7, \qquad -0.3 \le \kappa \le 0.3, \qquad 1.5 \le \tan\beta \le 2.5,$$
$$100\ \text{GeV} \le |\mu_{\text{eff}}| \le 185\ \text{GeV}. \tag{5.1}$$

In this parameter region the second lightest Higgs boson H_2 is SM-like.[12] The heavier CP-even and CP-odd Higgs bosons, H_3 and A_2, are predominantly a superposition of the components of the Higgs doublets (MSSM-like states). The lightest scalar and pseudoscalar Higgs states, H_1 and A_1, are singlet dominated. In the following we will use the convenient notation:

(i) As before, h denotes the SM-like Higgs boson, and here $H_2 \equiv h$.
(ii) The doubletlike heavy Higgs bosons will be denoted as $H_3 \equiv H$ and $A_2 \equiv A$.
(iii) The singlet dominated lightest CP-even and CP-odd Higgs bosons are called $H_1 \equiv H_s$ and $A_1 \equiv A_s$, respectively.

[11]This part of the NMSSM parameter space is favored by low fine-tuning considerations for $\lambda > 0.55$. For a recent analysis see [8].

[12]In order to have $H_1 \equiv h$, higher μ_{eff} values than the ones chosen here would be required.

At tree-level the NMSSM with approximate Peccei-Quinn symmetry leads to a hierarchical structure of the Higgs spectrum which consists of the heaviest CP-even, the heaviest CP-odd and the charged Higgs bosons being almost degenerate. Their mass scale is set by $\mu_{\rm eff}\tan\beta$ [95]; hence,

$$M_H \approx M_A \approx M_{H^\pm} \approx \mu_{\rm eff}\tan\beta. \tag{5.2}$$

Since $|\kappa| < \lambda$, the masses of the singlet dominated CP-even and CP-odd Higgs states are smaller than $\mu_{\rm eff}\tan\beta$, with the upper bound given by

$$M_{A_s}^2 + 3M_{H_s}^2 \approx 12\left(\frac{\kappa}{\lambda}\mu_{\rm eff}\right)^2 + \Delta. \tag{5.3}$$

The additional contribution Δ will be quantified later. We now turn to the discussion of the discovery prospects for the Higgs spectrum in this set-up. In the part of the NMSSM parameter space that we are considering the almost degenerate heavy CP-even, CP-odd and charged Higgs bosons have masses below about 530 GeV, so that they should still be light enough to be observed at the 13 TeV LHC. Due to the substantial mixing, because of the large value of λ, between the SM-like Higgs state and the singlet dominated CP-even state the production cross sections of the lightest and second lightest CP-even Higgs states are in general large enough to produce these particles. In case the non-SM-like CP-even Higgs boson is almost a singlet it may still be produced via the decays of the heavier Higgs states, because of the large λ value. The same holds for the singlet-dominated lightest CP-odd Higgs state. We list in the Appendix the Higgs couplings involved in the Higgs-to-Higgs decays for the approximations made here. Their inspection gives information on the possible decays to be expected. In summary, all Higgs bosons of the natural NMSSM should in general be accessible, so that this scenario may be constrained at the next round of the LHC run.

We confront these approximate considerations with the results from our parameter scan in the subspace given by the natural NMSSM. The approximate $\mu_{\rm eff}\tan\beta$ mass value of the heavy Higgs states is slightly modified by loop corrections and they range between about 230 and 530 GeV. Taking into account higher order mass corrections the mass relation for the singlet states, Eq. (5.3), approximately holds if we choose $\Delta = 18690\ (\text{GeV})^2$. Furthermore, H and A are indeed dominantly doubletlike, while the lightest CP-even and CP-odd states H_s and A_s are singletlike. The CP-even singlet mass ranges between 27 and 117 GeV. The upper bound is given by the LHC exclusion limits on the one hand and the fact, that the 125 GeV Higgs boson must be SM-like, on the other hand. The CP-odd singlet mass lies between 29 and 300 GeV. Note that for H_s there are only a few points below 62 GeV and for A_s even less. The reason is that the SM-like h could decay into these final states and this would drive its reduced signal rates away from the measured values. Thus the natural NMSSM scenario implies the existence of a CP-even Higgs state H_s that tends to have a mass of $62\ \text{GeV} \lesssim M_{H_s} \lesssim 117\ \text{GeV}$, and of a CP-odd state A_s with $62\ \text{GeV} \lesssim M_{A_s} \lesssim 300\ \text{GeV}$.

We find that the H and A gluon fusion production cross sections range between ~7.5 pb (H), respectively, ~4.5 pb (A) at the low mass end and 0.6–0.8 pb at the high mass end, as shown in Fig. 10. As H has a small up-type component admixture, the cross section cannot be as large as in the SM for a Higgs boson of same mass. Still, in the natural NMSSM, the size of the cross sections in most cases is large enough to discover these particles in the standard final states like $b\bar{b}$ (modulo the challenge due to large backgrounds), $\tau\tau$ or even $t\bar{t}$. For H the massive gauge boson final states add to the search channels. As can be inferred from Figs. 9 of the enlarged scan, in the mass and $\tan\beta$ range we consider here, for most of the cases the production rates in the various final states are above 1 fb, depending on the final state even well above 1 fb.

Figure 11 shows the gluon fusion production cross sections for H_s (left) and A_s (right) at a c.m. energy of

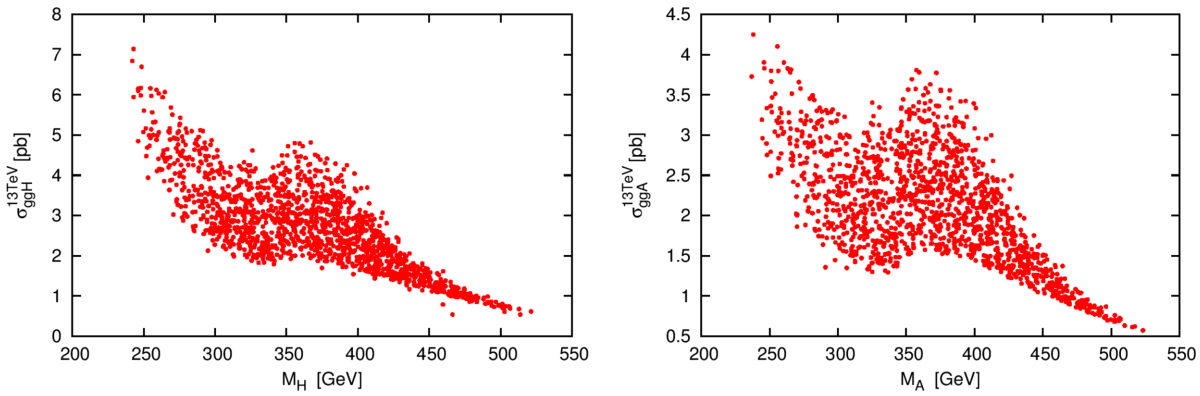

FIG. 10 (color online). The gluon fusion production cross section at $\sqrt{s} = 13$ TeV for H (left) and A (right) as a function of their mass.

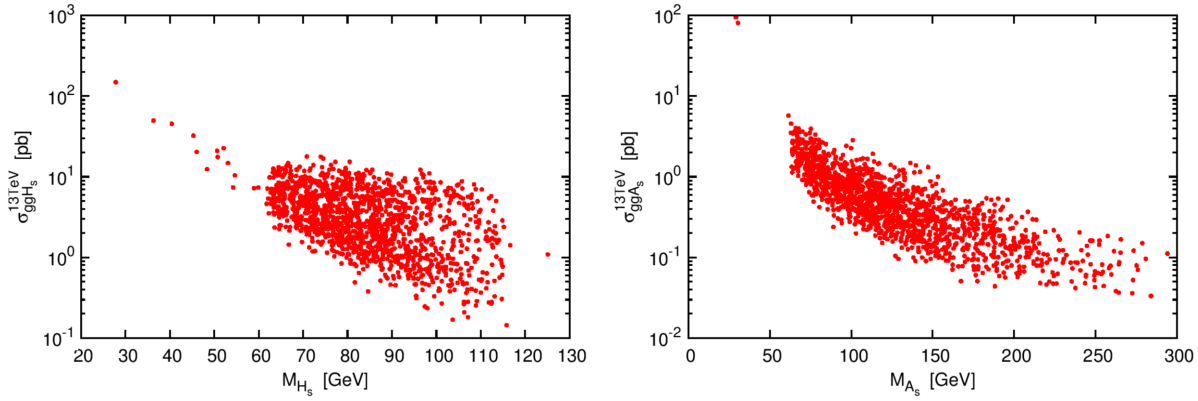

FIG. 11 (color online). The gluon fusion production cross section at $\sqrt{s} = 13$ TeV for H_s (left) and A_s (right) as a function of their mass.

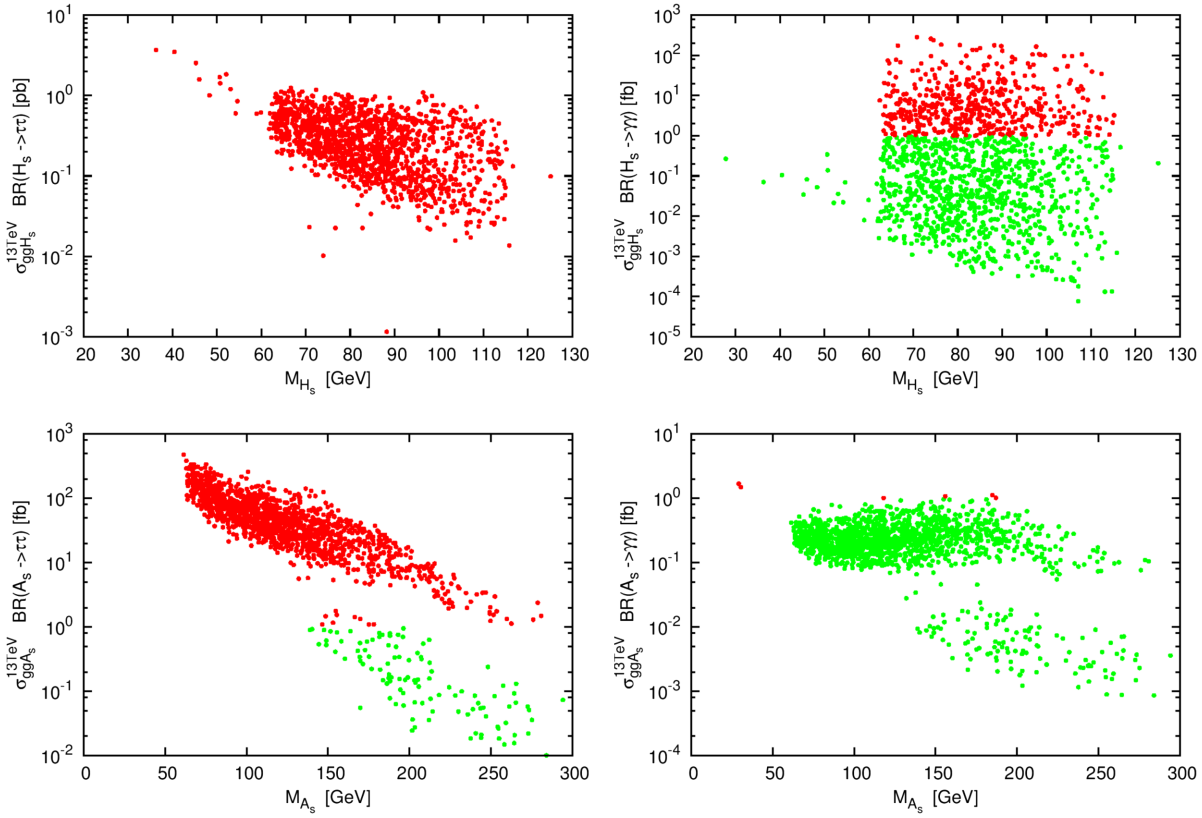

FIG. 12 (color online). Production rates for H_s (upper) and A_s (lower) production in gluon fusion with subsequent decay into the $\tau\tau$ (left) and $\gamma\gamma$ (right) final states as a function of the involved singlet mass, at $\sqrt{s} = 13$ TeV. Red (green) points mark cross sections above (below) 1 fb.

$\sqrt{s} = 13$ TeV. For small H_s masses the cross sections are rather large with several tens of pb. Above ~90 GeV the maximum values are below 10 pb and can go down to $\mathcal{O}(0.1$ pb). With the exception of cross sections around 100 pb for very small A_s masses, the pseudoscalar production cross sections reach at most 6 pb in the lower mass range. However, already for masses around 150 GeV, the cross sections can be as small as 0.1 pb.

If the light Higgs bosons are very singletlike their production rates may become very small, in particular in the pseudoscalar case, as can be inferred from Figs. 12, which show the production in the photon and τ-pair final states.[13] In this case and/or if the production rates also for the heavy Higgs bosons are small, further alternative production channels should be exploited to increase the discovery potential of the entire Higgs spectrum. This is

[13]For the b-quark pair final state, the cross sections, not shown here, are always above 1 fb and can reach values of up to $\mathcal{O}(10$ pb), for very light H_s even several tens of pb.

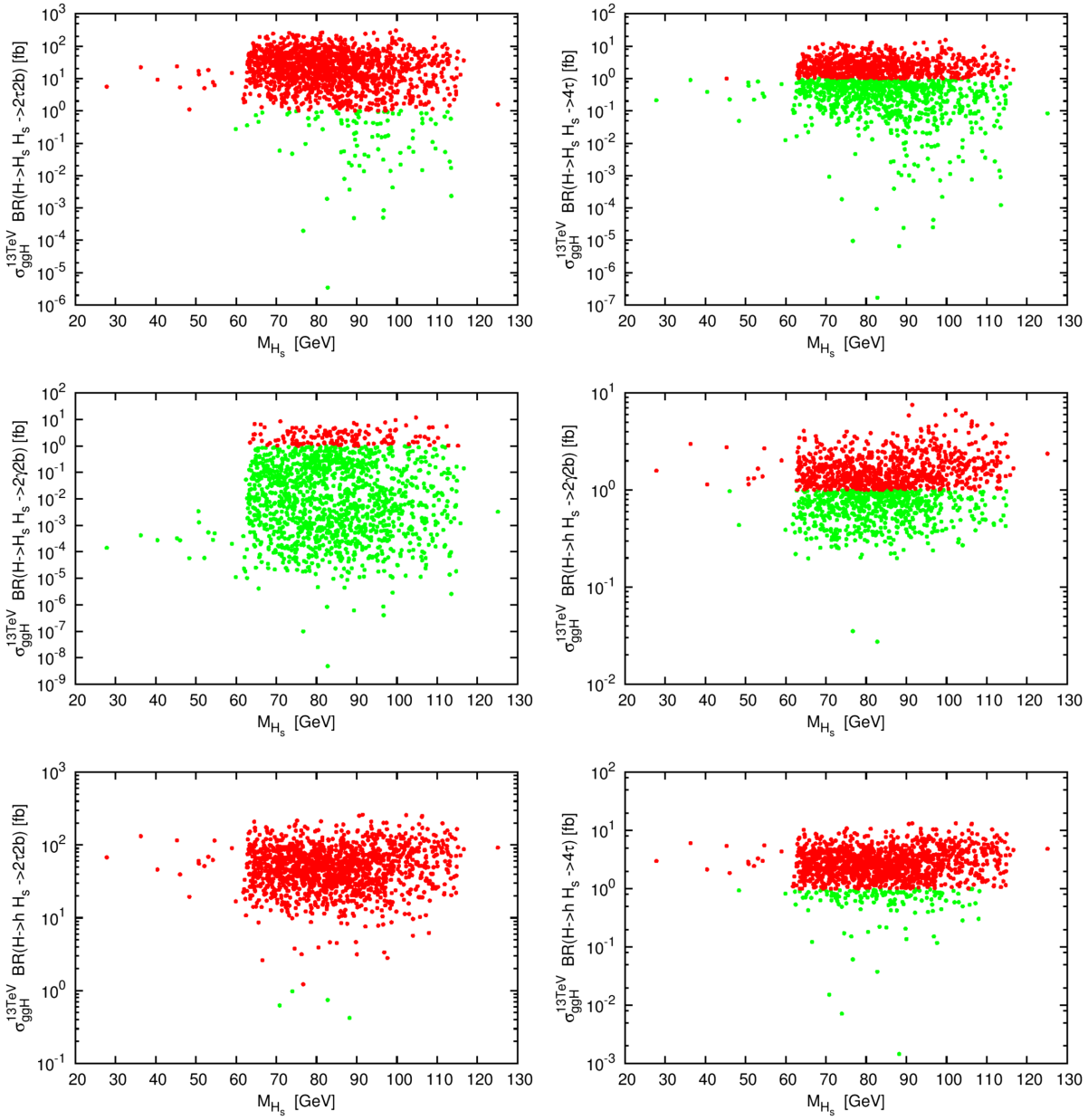

FIG. 13 (color online). Cross sections for H_sH_s production (upper two rows) and hH_s production (lower two rows) from H decay, in the $(2\tau)(2b)$ (upper/lower left), 4τ (upper/lower right) and $(2\gamma)(2b)$ (middle) final states at $\sqrt{s} = 13$ TeV as a function of the singlet mass M_{H_s}. Red (green) points mark cross sections above (below) 1 fb.

subject to the following two subsections, that discuss Higgs-to-Higgs and Higgs-to-gauge-Higgs decays in the natural NMSSM.

A. Singletlike Higgs production from Higgs-to-Higgs decays

In case not all neutral Higgs bosons can be discovered in direct production with subsequent decay, alternative search channels might be given by production from SUSY states decaying into Higgs bosons, or they may be searched for in Higgs decays into a Higgs and gauge boson pair as well as in Higgs-to-Higgs decays, i.e.

$$\sigma(gg \to \phi_i) \times BR(\phi_i \to \phi_j\phi_k) \times BR(\phi_j \to XX) \times BR(\phi_k \to YY), \tag{5.4}$$

where $\phi_{i,j,k}$ generically denotes one of the five neutral Higgs bosons[14] and with $M_{\phi_i} > M_{\phi_j} + M_{\phi_k}$.

The production rates for singlet Higgs pairs H_sH_s and a singlet plus SM-like Higgs, H_sh, from the heavy CP-even Higgs boson H are shown in Figs. 13, including their

[14]Of course in Eq. (5.4) only these Higgs-to-Higgs decays are considered that are allowed by the quantum numbers.

subsequent decay into SM particles. Red (green) points refer to cross sections above (below) 1 fb. The figures show, that in the $(2\tau)(2b)$ final state the cross sections are above 1 fb, with the exception of a few points in the H_sH_s production. They can even reach values of several hundred fb. The 4τ final state is suppressed by a factor 10 compared to the former, but still a good fraction of scenarios, in particular for hH_s production, reaches cross sections larger than 1 fb. As expected, the $(2\gamma)(2b)$ final state rates are smaller, but also here we have scenarios with rates exceeding the fb level. In principle H could also decay into a pair of pseudoscalar singlets. However, in this case all the decay rates turned out to be tiny so that we do not display them here.

Singlet Higgs bosons can also be produced from heavy pseudoscalar decays into H_sA_s or hA_s. The production rates into the $(2\tau)(2b)$, 4τ and $(2\gamma)(2b)$ final states are shown in Figs. 14. Again we have a non-negligible fraction of scenarios that lead to rates exceeding 1 fb in the pure fermionic final states. In the $(2\gamma)(2b)$ final states the majority of points is below 1 fb.

Finally note, that we have shown here only the simplest final state combinations. As will be evident from the benchmark discussion, however, there can also be more

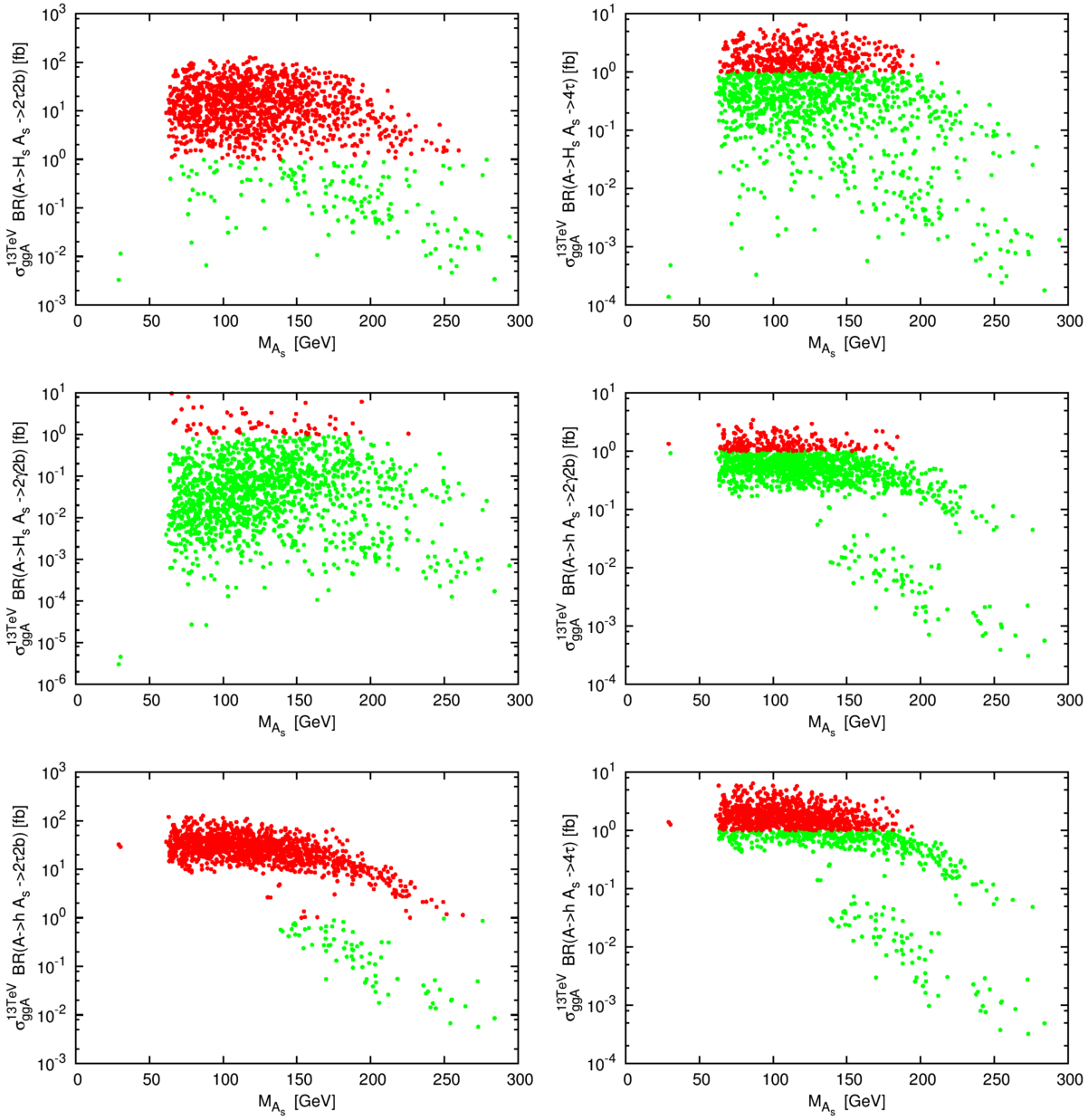

FIG. 14 (color online). Cross sections for A_sH_s production (upper two rows) and hA_s production (lower two rows) from A decay, in the $(2\tau)(2b)$ (upper/lower left), 4τ (upper/lower right) and $(2\gamma)(2b)$ (middle) final states at $\sqrt{s} = 13$ TeV as a function of the singlet mass M_{A_s}. Red (green) points mark cross sections above (below) 1 fb.

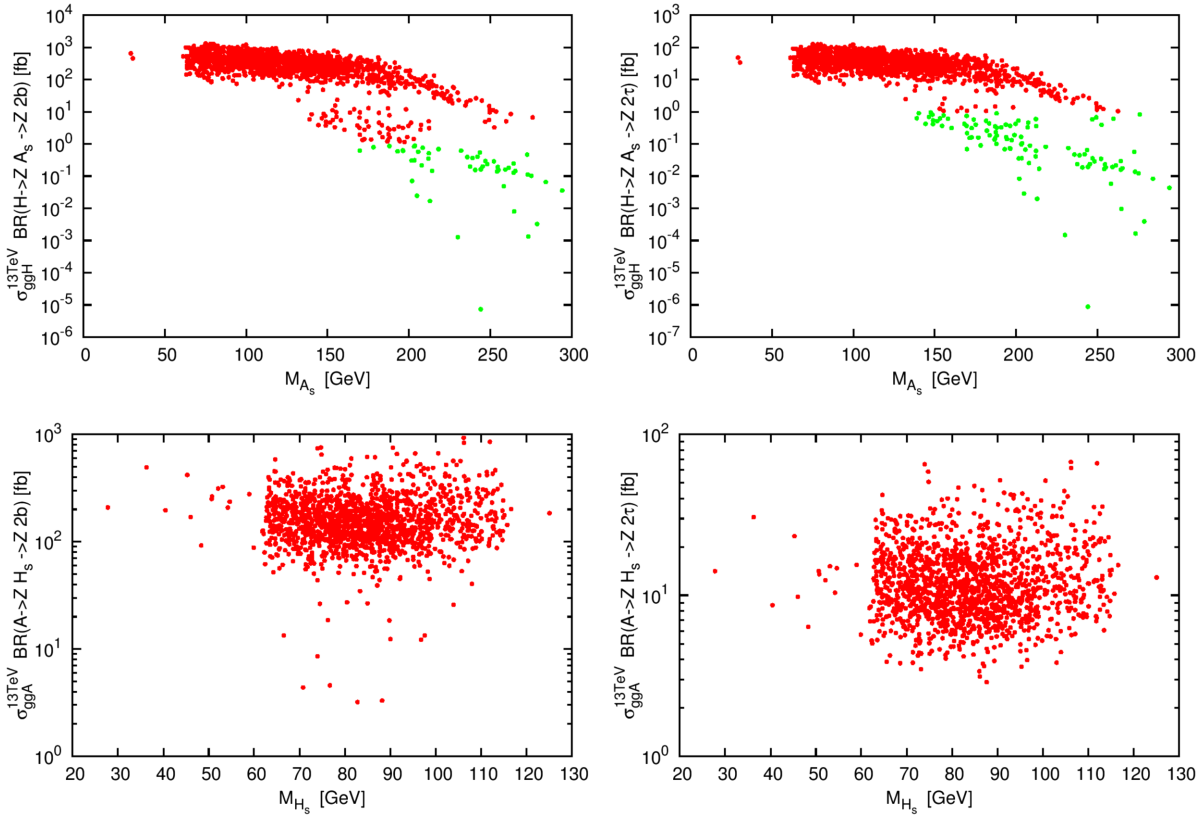

FIG. 15 (color online). Cross sections for ZA_s production from H decay (upper) and for ZH_s production from A decay (lower) in the $Z + 2b$ (left) and $Z + 2\tau$ (right) final state, respectively, as a function of the involved singlet mass, at $\sqrt{s} = 13$ TeV. Red (green) points mark cross sections above (below) 1 fb.

complicated and more exotic final states arising from two Higgs-to-Higgs decays in one decay chain.

B. Singletlike Higgs production from Higgs-to-gauge-Higgs decays

Singlet Higgs boson production is also possible via heavy Higgs decays into a singlet Higgs and a massive gauge boson. While these cross sections do not involve trilinear Higgs couplings, they lead to interesting decay rates. The cross sections for the $H \to ZA_s$ and $A \to ZH_s$ decays in the $Z + 2b$ and $Z + 2\tau$ final states are shown in Fig. 15. The rates will go down by another factor 30 due to the Z boson decay into fermions. Still, almost all parameter points have cross sections above 1 fb up to pb in the $Z + 2b$ final state, reduced by a factor 10 in the $Z + 2\tau$ final state, and with the exception of some points in the chain via the ZA_s final state for pseudoscalar singlet masses above ~150 GeV. These decay chains can hence be used as additional and complementary production channels for singlet Higgs bosons.

In summary, in general the complete Higgs spectrum of the natural NMSSM should be accessible at the high-energy LHC by exploiting the entity of Higgs production channels through direct production in gluon fusion[15] with subsequent decay into SM particles and the production from heavy Higgs boson decays into lighter Higgs pairs and/or Higgs plus gauge boson final states. Decays of heavy SUSY particles into lighter Higgs bosons, not discussed here, may possibly add to the discovery contours. This part of the NMSSM parameter space will therefore either strongly be constrained at the next LHC run to come, or lead to the discovery of beyond the SM physics revealed by the Higgs sector.

VI. BENCHMARKS FOR HIGGS-TO-HIGGS DECAYS

Higgs decays, as given in Eq. (5.4), into Higgs pairs that subsequently decay into SM particles are interesting for the discovery of the heavier Higgs boson ϕ_i provided its production cross section is large enough and the branching ratio into the lighter Higgs pair dominates over its branching ratios into the SM final states. For the lighter Higgs bosons ϕ_j, ϕ_k this production mechanism becomes interesting in

[15]We remind the reader that for simplification we only took into account the dominant gluon fusion production. In addition to this also the other LHC production mechanisms will contribute and even ameliorate the discovery prospects.

case their direct production is strongly suppressed due to them being very singletlike. Furthermore, Higgs-to-Higgs decays are interesting in themselves as they give access to the trilinear Higgs self-couplings, which can then be used to reconstruct the Higgs potential as the last step in the experimental verification of the Higgs mechanism [96].

In this section, we concentrate on Higgs-to-Higgs decays and present exemplary scenarios that are compatible with all constraints discussed above and that arise from our scan of the parameter space defined in Eqs. (3.1)–(3.7), i.e. not restricted to the natural NMSSM. The presented scenarios not only lead to sufficiently large cross sections for double Higgs production from heavier Higgs decays but some of them also entail exotic multiphoton and/or multifermion final states. The possibility of such final states should be taken into consideration by the experiments in order not to miss possible Higgs signatures, that can appear in multi-Higgs models like the NMSSM without particular fine-tuning of the parameters. We also include scenarios featuring a light CP-even Higgs boson with a mass below 10 GeV. The presented scenarios highlight specific features of NMSSM Higgs decay chains and can be viewed as benchmark scenarios for future LHC searches.

In the following we will again use the convenient notation introduced in section 5. Note, however, that the SM-like Higgs boson h can now be H_1 or H_2. The more doubletlike scalar H can be given by H_2 or H_3, depending on the scenario. The pseudoscalar doublet state A, as before, is given by A_2, and the singletlike CP-odd A_s by A_1. The singletlike scalar H_s, however, can be H_1, H_2 or even H_3.

The benchmark scenarios that we present can be classified as follows:

(A) $H_2 = h$, $H_1 = H_s$, $\tan\beta$ small, light spectrum $\lesssim$350 GeV: The scenarios A are characterized by the second lightest Higgs being SM-like, the lightest Higgs boson singletlike and small $\tan\beta$. The overall spectrum is rather light with maximal Higgs mass values of $M_H = 341$ GeV and $M_A = 347$ GeV.

A.1: The CP-odd singlet is close in mass to the SM-like Higgs with $M_{A_s} = 119$ GeV. The heavy Higgs bosons have masses around 341 and 347 GeV.

A.2: The CP-odd singlet is light with $M_{A_s} = 79$ GeV, the heavy Higgs bosons with masses around 326 GeV are somewhat lighter than in scenario A.1.

(B) $H_1 = h$, $H_2 = H_s$, $\tan\beta$ small: The scenarios B are characterized by the lightest Higgs being SM-like, the second lightest Higgs boson singletlike and small $\tan\beta$.

B.1: The CP-odd singlet is light with $M_{A_s} = 73$ GeV and the overall spectrum as well with the heavy H mass of 323 GeV and $M_A = 312$ GeV.

B.2: The pseudoscalar singlet with $M_{A_s} = 107$ GeV is still lighter than the SM-like Higgs, but the overall spectrum is heavier with $M_H = 556$ GeV and $M_A = 578$ GeV.

B.3: The singlet mass $M_{A_s} = 133$ GeV is now heavier than M_h. The maximum mass is given by $M_H = 463$ GeV, closely followed by $M_A = 457$ GeV.

(C) $\tan\beta > 5$: Here we explicitly chose a scenario where $\tan\beta = 17$ is large. The lightest Higgs boson is SM-like $H_1 = h$. The spectrum is peculiar in the sense that the heavy scalar with a mass of ~3.5 TeV is very heavy. Additionally, H_3 is singletlike. The heavy pseudoscalar and second lightest scalar are doubletlike with masses of $\mathcal{O}(600$ GeV$)$. The pseudoscalar singlet is much heavier than h, $M_{A_s} = 312$ GeV.

(D) The SM-like h, given by H_2, can decay into Higgs pairs: The scenarios D allow for decays of the SM-like Higgs h into lighter singlet Higgs pairs.

D.1: The CP-even singlet is very light, $M_{H_s} < 10$ GeV, and h decays into CP-even singlet pairs are non-negligible. The pseudoscalar singlet is heavier than 125 GeV, and heavy Higgs bosons have masses up to 793 GeV. The $\tan\beta$ value is small and below 5.

D.2: Here the CP-odd singlet is the lightest Higgs, and the SM-like Higgs h decays into A_s pairs. The scalar singlet H_s with 112 GeV is now closer in mass to h. The heavy Higgs masses are very large and of $\mathcal{O}(1.3$ TeV$)$. We have a medium $\tan\beta = 6.4$.

In all scenarios the lightest pseudoscalar is singletlike.

In the subsequent subsections the details on these benchmark scenarios will be given. The discovery prospects of the various Higgs bosons shall be highlighted with particular focus on the Higgs-to-Higgs decays and the related signatures.

A. Scenarios A - $H_2 \equiv h$ and small $\tan\beta$

The NMSSM-specific and soft SUSY breaking parameters defining scenarios A.1 and A.2 are given in Table III and IV, respectively. The relevant NMSSM Higgs signal rates are summarized in Table V for A.1 and Table VI for A.2. They feature a SM-like Higgs boson given by the next-to-lightest CP-even Higgs. In both scenarios the couplings of the singlets H_s and A_s to gluons amount to $\mathcal{O}(10$–$20\%)$ of the corresponding SM Higgs coupling of same mass leading to gluon fusion production cross sections of 1–2.4 pb. As the $b\bar{b}$ final state is difficult to detect, they could be searched for in $\tau\tau$ or even $\gamma\gamma$ final states. The heavy Higgs bosons H and A are produced with $\mathcal{O}(4$ pb$)$ cross sections and have sizeable decay rates into Higgs pairs involving A_s and H_s, and also into Z and a Higgs singlet, so that alternative search channels are given by Higgs cascade decays.

In scenario A.1 the H branching ratios both into H_sH_s and hH_s are larger than 10% and into ZA_s even 25%. This leads to interesting final states with b-quark and τ-pairs, 4τ's or even $(b\bar{b})(\gamma\gamma)$. The $4b$ final state may be difficult to exploit due to the large background. The pseudoscalar A

TABLE III. The parameters defining scenario A.1, together with the Higgs boson masses, singlet components and reduced signal rates of h.

A.1 (Point ID 3877)	Scenario		
$M_{H_1}, M_{H_2}, M_{H_3} = M_{H_s}, M_h, M_H$	90.3 GeV	126.8 GeV	341.3 GeV
$M_{A_1}, M_{A_2} = M_{A_s}, M_A$	118.5 GeV	346.7 GeV	
$\lvert S_{H_1 h_s}\rvert^2, \lvert P_{A_1 a_s}\rvert^2$	0.97	0.94	
$\mu_{\tau\tau}$, μ_{bb}	1.09	1.08	
μ_{ZZ}, μ_{WW}, $\mu_{\gamma\gamma}$	0.85	0.85	0.88
$\tan\beta$, λ, κ	1.66	0.64	0.11
A_λ, A_κ, μ_{eff}	338.0 GeV	−71.2 GeV	162.8 GeV
A_t, A_b, A_τ	181.1 GeV	−1530.0 GeV	87.2 GeV
M_1, M_2, M_3	440.0 GeV	813.7 GeV	1710.2 GeV
$M_{Q_3} = M_{t_R}$, M_{b_R}	1827.5 GeV	3 TeV	
$M_{L_3} = M_{\tau_R}$, M_{SUSY}	1663.7 GeV	3 TeV	

TABLE IV. The parameters defining scenario A.2, together with the Higgs boson masses, singlet components and reduced signal rates of h.

A.2 (Point ID 2212)	Scenario		
M_{H_s}, M_h, M_H	98.6 GeV	125.6 GeV	325.9 GeV
M_{A_s}, M_A	78.6 GeV	325.5 GeV	
$\lvert S_{H_1 h_s}\rvert^2, \lvert P_{A_1 a_s}\rvert^2$	0.89	0.96	
$\mu_{\tau\tau}$, μ_{bb}	1.05	0.93	
μ_{ZZ}, μ_{WW}, $\mu_{\gamma\gamma}$	0.86	0.87	0.90
$\tan\beta$, λ, κ	1.69	0.56	0.12
A_λ, A_κ, μ_{eff}	−259.2 GeV	−22.8 GeV	−147.4 GeV
A_t, A_b, A_τ	1927.4 GeV	−948.9 GeV	1621.4 GeV
M_1, M_2, M_3	755.9 GeV	646.7 GeV	2424.9 GeV
$M_{Q_3} = M_{t_R}$, M_{b_R}	2468.3 GeV	3 TeV	
$M_{L_3} = M_{\tau_R}$, M_{SUSY}	1623.0 GeV	3 TeV	

decays with a branching ratio of 0.14 into hA_s and less frequently into H_sA_s and ZH_s ($\text{BR}(A \to H_sA_s) = 0.085$, $\text{BR}(A \to ZH_s) = 0.047$). Still the rates are large enough to provide discovery channels for the singlets. All these cascade decays of course also add to the discovery channels of the heavy H and A themselves.

In contrast to scenario A.1, in A.2 the decay of the heavy H into H_sH_s is not interesting, instead the branching ratio into hH_s is almost doubled compared to A.1, and also the one into ZA_s is somewhat enhanced. As for the A decays into hA_s and ZH_s, they are a factor 2.6 larger and the one into H_sA_s only half as large compared to A.1. Correspondingly the final state rates are changed.

These two scenarios are examples of an NMSSM Higgs spectrum which is rather light and where all Higgs bosons can be discovered, both directly or in Higgs-to-Higgs or Higgs-to-gauge-Higgs decays. They also show the importance of looking into photon final states at mass values below 125 GeV. Furthermore, the Higgs cascade decays give access to the trilinear Higgs self-couplings $\lambda_{HH_sH_s}$, λ_{HH_sh}, λ_{AA_sh} and $\lambda_{AA_sH_s}$. Finally, the heavy scalar and pseudoscalar also have sizeable rates into a pair of two lightest neutralinos. Though this final state leads to missing energy signatures and does not allow for the mass reconstruction it adds to possible search channels.

B. Scenarios B - $H_1 \equiv h$ and small $\tan\beta$

In the scenarios B it is the lightest Higgs boson that is SM-like.

(B.1) Singletlike A_1 production from heavy Higgs decays: The definition of scenario B.1 is given in Table VII and the signal rates in Table VIII. The scenario is very special as it not only involves a very singletlike lightest pseudoscalar $A_1 \equiv A_s$, but this also has a large branching ratio into photons, $\text{BR}(A_s \to \gamma\gamma) = 0.84$. Together with large Higgs-to-Higgs branching ratios for H_s and H, $\text{BR}(H_s \to A_sA_s) = 0.97$ and $\text{BR}(H \to hH_s) = 0.51$, this leads to spectacular signatures with multiphoton and/or multi-b as well multi-τ final states.

In detail, due to the singlet nature of A_s its gluon fusion production cross section is extremely small with only 0.08 fb, so that alternative production mechanisms must be exploited. The H_s coupling to gluons is large enough to

TABLE V. The signal rates for A.1.

A.1 (Point ID 3877)	Signal rates
$\sigma(ggH_s)$	2.37 pb
$\sigma(ggH_s)\mathrm{BR}(H_s \to b\bar{b})$	2.04 pb
$\sigma(ggH_s)\mathrm{BR}(H_s \to \tau\tau)$	204.82 fb
$\sigma(ggH_s)\mathrm{BR}(H_s \to \gamma\gamma)$	2.74 fb
$\sigma(ggH)$	4.29 pb
$\sigma(ggH)\mathrm{BR}(H \to b\bar{b})$	40.88 fb
$\sigma(ggH)\mathrm{BR}(H \to \tau\tau)$	5.10 fb
$\sigma(ggH)\mathrm{BR}(H \to WW)$	49.13 fb
$\sigma(ggH)\mathrm{BR}(H \to ZZ)$	22.41 fb
$\sigma(ggH)\mathrm{BR}(H \to \tilde{\chi}_1^0\tilde{\chi}_1^0)$	1.27 pb
$\sigma(ggH)\mathrm{BR}(H \to H_sH_s)$	458.74 fb
$\sigma(ggH)\mathrm{BR}(H \to H_sH_s \to bb+bb)$	341.12 fb
$\sigma(ggH)\mathrm{BR}(H \to H_sH_s \to bb+\tau\tau)$	68.34 fb
$\sigma(ggH)\mathrm{BR}(H \to H_sH_s \to \tau\tau+\tau\tau)$	3.42 fb
$\sigma(ggH)\mathrm{BR}(H \to H_sH_s \to bb+\gamma\gamma)$	0.92 fb
$\sigma(ggH)\mathrm{BR}(H \to hH_s)$	505.60 fb
$\sigma(ggH)\mathrm{BR}(H \to hH_s \to bb+bb)$	274.92 fb
$\sigma(ggH)\mathrm{BR}(H \to hH_s \to bb+\tau\tau)$	56.46 fb
$\sigma(ggH)\mathrm{BR}(H \to hH_s \to \tau\tau+\tau\tau)$	2.90 fb
$\sigma(ggH)\mathrm{BR}(H \to hH_s \to bb+\gamma\gamma)$	1.34 fb
$\sigma(ggH)\mathrm{BR}(H \to ZA_s)$	1.07 pb
$\sigma(ggH)\mathrm{BR}(H \to ZA_s \to ll+bb)$	31.67 fb
$\sigma(ggH)\mathrm{BR}(H \to ZA_s \to \tau\tau+bb)$	46.59 fb
$\sigma(ggH)\mathrm{BR}(H \to ZA_s \to \tau\tau+\tau\tau)$	3.32 fb
$\sigma(ggA_s)$	914.07 fb
$\sigma(ggA_s)\mathrm{BR}(A_s \to b\bar{b})$	804.77 fb
$\sigma(ggA_s)\mathrm{BR}(A_s \to \tau\tau)$	84.15 fb
$\sigma(ggA_s)\mathrm{BR}(A_s \to \gamma\gamma)$	0.36 fb
$\sigma(ggA)$	3.36 pb
$\sigma(ggA)\mathrm{BR}(A \to t\bar{t})$	1.43 pb
$\sigma(ggA)\mathrm{BR}(A \to \tilde{\chi}_1^0\tilde{\chi}_1^0)$	686.00 fb
$\sigma(ggA)\mathrm{BR}(A \to hA_s)$	472.37 fb
$\sigma(ggA)\mathrm{BR}(A \to hA_s \to bb+bb)$	262.24 fb
$\sigma(ggA)\mathrm{BR}(A \to hA_s \to \tau\tau+bb)$	55.00 fb
$\sigma(ggA)\mathrm{BR}(A \to hA_s \to \tau\tau+\tau\tau)$	2.88 fb
$\sigma(ggA)\mathrm{BR}(A \to hA_s \to WW+bb)$	85.39 fb
$\sigma(ggA)\mathrm{BR}(A \to hA_s \to \gamma\gamma+bb)$	1.04 fb
$\sigma(ggA)\mathrm{BR}(A \to H_sA_s)$	285.76 fb
$\sigma(ggA)\mathrm{BR}(A \to H_sA_s \to bb+bb)$	216.95 fb
$\sigma(ggA)\mathrm{BR}(A \to H_sA_s \to \tau\tau+bb)$	44.42 fb
$\sigma(ggA)\mathrm{BR}(A \to H_sA_s \to \tau\tau+\tau\tau)$	2.27 fb
$\sigma(ggA)\mathrm{BR}(A \to H_sA_s \to \gamma\gamma+bb)$	0.39 fb
$\sigma(ggA)\mathrm{BR}(A \to ZH_s)$	158.13 fb
$\sigma(ggA)\mathrm{BR}(A \to ZH_s \to ll+b\bar{b})$	4.59 fb
$\sigma(ggA)\mathrm{BR}(A \to ZH_s \to \tau\tau+b\bar{b})$	6.66 fb
$\sigma(ggA)\mathrm{BR}(A \to ZH_s \to \tau\tau+\tau\tau)$	0.46 fb

TABLE VI. The signal rates for A.2.

A.2 (Point ID 2212)	Signal rates
$\sigma(ggH_s)$	2.36 pb
$\sigma(ggH_s)\mathrm{BR}(H_s \to b\bar{b})$	2.12 pb
$\sigma(ggH_s)\mathrm{BR}(H_s \to \tau\tau)$	214 fb
$\sigma(ggH_s)\mathrm{BR}(H_s \to \gamma\gamma)$	0.4 fb
$\sigma(ggH)$	4.34 pb
$\sigma(ggH)\mathrm{BR}(H \to bb)$	66.98 fb
$\sigma(ggH)\mathrm{BR}(H \to \tau\tau)$	8.29 fb
$\sigma(ggH)\mathrm{BR}(H \to WW)$	151.38 fb
$\sigma(ggH)\mathrm{BR}(H \to ZZ)$	68.47 fb
$\sigma(ggH)\mathrm{BR}(H \to \tilde{\chi}_1^0\tilde{\chi}_1^0)$	854.09 fb
$\sigma(ggH)\mathrm{BR}(H \to hH_s)$	899.34 fb
$\sigma(ggH)\mathrm{BR}(H \to hH_s \to bb+bb)$	506.58 fb
$\sigma(ggH)\mathrm{BR}(H \to hH_s \to bb+\tau\tau)$	104.25 fb
$\sigma(ggH)\mathrm{BR}(H \to hH_s \to \tau\tau+\tau\tau)$	5.36 fb
$\sigma(ggH)\mathrm{BR}(H \to hH_s \to bb+\gamma\gamma)$	2.02 fb
$\sigma(ggH)\mathrm{BR}(H \to hH_s \to WW+b\bar{b})$	161.89 fb
$\sigma(ggH)\mathrm{BR}(H \to ZA_s)$	1.43 pb
$\sigma(ggH)\mathrm{BR}(H \to ZA_s \to ll+b\bar{b})$	43.41 fb
$\sigma(ggH)\mathrm{BR}(H \to ZA_s \to \tau\tau+b\bar{b})$	62.10 fb
$\sigma(ggH)\mathrm{BR}(H \to ZA_s \to \tau\tau+\tau\tau)$	4.15 fb
$\sigma(ggA_s)$	1.36 pb
$\sigma(ggA_s)\mathrm{BR}(A_s \to b\bar{b})$	1.22 pb
$\sigma(ggA_s)\mathrm{BR}(A_s \to \tau\tau)$	116.8 fb
$\sigma(ggA_s)\mathrm{BR}(A_s \to \gamma\gamma)$	0.3 fb
$\sigma(ggA)$	3.04 pb
$\sigma(ggA)\mathrm{BR}(A \to \tilde{\chi}_1^0\tilde{\chi}_1^0)$	1.16 pb
$\sigma(ggA)\mathrm{BR}(A \to hA_s)$	1.13 pb
$\sigma(ggA)\mathrm{BR}(A \to hA_s \to bb+bb)$	640.74 fb
$\sigma(ggA)\mathrm{BR}(A \to hA_s \to bb+\tau\tau)$	128.37 fb
$\sigma(ggA)\mathrm{BR}(A \to hA_s \to \tau\tau+\tau\tau)$	6.42 fb
$\sigma(ggA)\mathrm{BR}(A \to hA_s \to bb+WW)$	203.85 fb
$\sigma(ggA)\mathrm{BR}(A \to hA_s \to bb+\gamma\gamma)$	2.60 fb
$\sigma(ggA)\mathrm{BR}(A \to H_sA_s)$	131.49 fb
$\sigma(ggA)\mathrm{BR}(A \to H_sA_s \to bb+bb)$	106.17 fb
$\sigma(ggA)\mathrm{BR}(A \to H_sA_s \to bb+\tau\tau)$	20.87 fb
$\sigma(ggA)\mathrm{BR}(A \to H_sA_s \to \tau\tau+\tau\tau)$	1.02 fb
$\sigma(ggA)\mathrm{BR}(A \to ZH_s)$	378.42 fb
$\sigma(ggA)\mathrm{BR}(A \to ZH_s \to ll+b\bar{b})$	11.43 fb
$\sigma(ggA)\mathrm{BR}(A \to ZH_s \to \tau\tau+b\bar{b})$	16.63 fb
$\sigma(ggA)\mathrm{BR}(A \to ZH_s \to \tau\tau+\tau\tau)$	1.16 fb

lead to a sizeable cross section of 282 fb. (It is smaller by almost a factor 10 compared to the scenarios A because H_s here is the second lightest Higgs and hence the available phase space is smaller.) As H_s has a large branching ratio into A_s pairs and A_s itself into photon pairs, the thus produced four photon final state rate amounts to almost 200 fb. The heavy doublet Higgs H is produced in gluon fusion with 3.2 pb and its branching ratio into hH_s is 0.51. With the large H_s decay rate into A_sA_s this leads to very peculiar signatures with up to 6 photons in the final state. The largest rate is given by the $(4\gamma)(b\bar{b})$ signature with 712 fb. Additionally, we have A production in gluon fusion at 2.5 pb, which leads via the decay into H_sA_s ($\mathrm{BR}(A \to H_sA_s) = 0.21$) again to multiphoton final states with or without additional b-quark or τ-pairs. Here the 6γ final state even amounts to 302 fb. With a branching ratio $\mathrm{BR}(A \to ZH_s) = 0.22$ also this decay leads to interesting final states with e.g. $(4\gamma)(b\bar{b})$ production at 58 fb. Finally, also the decay into hA_s may be exploited in its $(\gamma\gamma)(b\bar{b})$ final state with a cross section of 16 fb. These and more

TABLE VII. The parameters defining scenario B.1, together with the Higgs boson masses, singlet components and reduced signal rates of h.

B.1 (Point ID Poi2a)	Scenario		
M_h, M_{H_s}, M_H	124.6 GeV	181.7 GeV	322.6 GeV
M_{A_s}, M_A	72.5 GeV	311.7 GeV	
$\lvert S_{H_2h_s}\rvert^2, \lvert P_{A_1a_s}\rvert^2$	0.90	1	
$\mu_{\tau\tau}$, μ_{bb}	1.54	1.01	
μ_{ZZ}, μ_{WW}, $\mu_{\gamma\gamma}$	0.93	0.93	1.01
$\tan\beta, \lambda, \kappa$	1.9	0.628	0.354
$A_\lambda, A_\kappa, \mu_{\text{eff}}$	251.2 GeV	53.8 GeV	158.9 GeV
M_1, M_2, M_3	890 GeV	576 GeV	1219 GeV
A_t, A_b, A_τ	1555 GeV	−1005 GeV	−840 GeV
$M_{Q_3} = M_{t_R}$, M_{b_R}	1075 GeV	1 TeV	
$M_{L_3} = M_{\tau_R}$, M_{SUSY}	530 GeV	2.5 TeV	

possible combinations and final states are summarized in Table VIII. It shows that in this scenario with a rather light overall spectrum, all Higgs bosons can be discovered, and that there are spectacular signatures possible that can be helpful for the discovery. Additionally, in the cascade decays the trilinear couplings $\lambda_{H_sA_sA_s}$, λ_{HH_sh}, $\lambda_{HA_sA_s}$, $\lambda_{AA_sH_s}$ and λ_{AA_sh} are accessible. Note finally, that the multiphoton (plus fermion) final states discussed here cannot occur in the MSSM and are unique to an extension beyond, as the NMSSM.

(B.2) Heavy Higgs spectrum: Scenario B.2, defined in Table IX is an example for a spectrum where it is challenging to find all NMSSM Higgs states. This is because of the heavier H and A with masses around 560 GeV, a not so light A_s as e.g. in scenario A.2 and a very singletlike H_s. The latter has a gluon fusion production cross section of 19 fb, leading to a $\tau\tau$ final state at only 0.3 fb, cf. Table X. The only alternative production via Higgs-to-Higgs decays is given by the $H \to hH_s$ decay leading to small 0.5 fb in the $(\tau\tau)(b\bar{b})$ final state. The pseudoscalar singlet A_s on the other hand has a larger gluon fusion production cross section now than in B.1 and can be searched for in standard final states. Additionally the decay of A into hA_s can be used to produce A_s in the $(\tau\tau)(b\bar{b})$ final state e.g. at 21 fb. Also the $H \to ZA_s \to (\tau\tau)(b\bar{b})$ production leading to 14 fb, may be used. Both H and A are heavy enough to decay into top pairs and may be discovered in these decay channels with rates into $t\bar{t}$ between 550 fb for A and 623 fb for H. In this scenario only the trilinear couplings λ_{HH_sh} and λ_{AA_sh} are accessible.

(B.3) Heavy Higgs spectrum, B.2 reversed: The scenario B.3, cf. Table XI, is reversed compared to B.2 in the sense that now $H_2 \equiv H_s$ is somewhat less singletlike and $A_1 \equiv A_s$ is very singletlike, so that here A_s production will be challenging. Its gluon fusion production cross section amounts only to 32 fb leading to a $\tau\tau$ rate of 3 fb as can be inferred from Table XII. It can also be produced in heavy A cascade decays via hA_s and H_sA_s. The former leads to 3.9 fb in the $(\tau\tau)(b\bar{b})$ final state, the latter to 1.7 fb. The singlet H_s now can be looked for in standard final states as e.g. $\tau\tau$ with 18 fb or with larger rates in gauge boson final states. It can also be produced from $A \to ZH_s$ decays. The heavy H and A again can decay into top pairs, at rates around 680 fb. The pseudoscalar doublet A

TABLE VIII. The signal rates for B.1.

B.1 (Point ID Poi2a)	Decay rates
$\sigma(ggH_s)$	282.37 fb
$\sigma(ggH_s)\text{BR}(H_s \to WW)$	5.09 fb
$\sigma(ggH_s)\text{BR}(H_s \to A_sA_s)$	274.75 fb
$\sigma(ggH_s)\text{BR}(H_s \to A_sA_s \to b\bar{b}+b\bar{b})$	5.87 fb
$\sigma(ggH_s)\text{BR}(H_s \to A_sA_s \to \gamma\gamma+b\bar{b})$	67.33 fb
$\sigma(ggH_s)\text{BR}(H_s \to A_sA_s \to \gamma\gamma+\gamma\gamma)$	193.22 fb
$\sigma(ggH)$	3.17 pb
$\sigma(ggH)\text{BR}(H \to WW)$	264.73 fb
$\sigma(ggH)\text{BR}(H \to ZZ)$	119.52 fb
$\sigma(ggH)\text{BR}(H \to b\bar{b})$	297.37 fb
$\sigma(ggH)\text{BR}(H \to \tau\tau)$	37.65 fb
$\sigma(ggH)\text{BR}(H \to \tilde{\chi}_1^0\tilde{\chi}_1^0)$	383.33 fb
$\sigma(ggH)\text{BR}(H \to \tilde{\chi}_1^+\tilde{\chi}_1^-)$	403.14 fb
$\sigma(ggH)\text{BR}(H \to hH_s)$	1.609 pb
$\sigma(ggH)\text{BR}(H \to hH_s \to bb+\tau\tau)$	1.44 fb
$\sigma(ggH)\text{BR}(H \to hH_s \to h+A_sA_s \to bb+4\gamma)$	712.47 fb
$\sigma(ggH)\text{BR}(H \to hH_s \to h+A_sA_s \to \gamma\gamma+4b)$	248.02 fb
$\sigma(ggH)\text{BR}(H \to hH_s \to h+A_sA_s \to \tau\tau+4\gamma)$	74.60 fb
$\sigma(ggH)\text{BR}(H \to hH_s \to h+A_sA_s \to \gamma\gamma+4\tau)$	2.47 fb
$\sigma(ggH)\text{BR}(H \to hH_s \to h+A_sA_s \to 6\gamma)$	2.69 fb
$\sigma(ggH)\text{BR}(H \to hH_s \to h+A_sA_s \to \tau\tau+\gamma\gamma+b\bar{b})$	49.55 fb
$\sigma(ggH)\text{BR}(H \to A_sA_s)$	5.59 fb
$\sigma(ggH)\text{BR}(H \to A_sA_s \to 4\gamma)$	3.93 fb
$\sigma(ggA_s)$	0.08 fb
$\sigma(ggA)$	2.51 pb
$\sigma(ggA)\text{BR}(A \to \tau\tau)$	14.42 fb
$\sigma(ggA)\text{BR}(A \to \tilde{\chi}_1^0\tilde{\chi}_1^0)$	963.87 fb
$\sigma(ggA)\text{BR}(A \to \tilde{\chi}_1^+\tilde{\chi}_1^-)$	273.57 fb
$\sigma(ggA)\text{BR}(A \to H_sA_s)$	525.56 fb
$\sigma(ggA)\text{BR}(A \to H_sA_s \to A_sA_s+A_s \to 6\gamma)$	301.58 fb
$\sigma(ggA)\text{BR}(A \to H_sA_s \to A_sA_s+A_s \to bb+4\gamma)$	157.64 fb
$\sigma(ggA)\text{BR}(A \to H_sA_s \to A_sA_s+A_s \to 4b+\gamma\gamma)$	27.47 fb
$\sigma(ggA)\text{BR}(A \to H_sA_s \to A_sA_s+A_s \to \tau\tau+4\gamma)$	14.99 fb
$\sigma(ggA)\text{BR}(A \to H_sA_s \to A_sA_s+A_s \to \tau\tau+bb+\gamma\gamma)$	5.22 fb
$\sigma(ggA)\text{BR}(A \to H_sA_s \to A_sA_s+A_s \to 4\tau+\gamma\gamma)$	0.25 fb
$\sigma(ggA)\text{BR}(A \to hA_s)$	29.96 fb
$\sigma(ggA)\text{BR}(A \to hA_s \to \gamma\gamma+b\bar{b})$	16.25 fb
$\sigma(ggA)\text{BR}(A \to hA_s \to \gamma\gamma+\tau\tau)$	1.70 fb
$\sigma(ggA)\text{BR}(A \to hA_s \to b\bar{b}+b\bar{b})$	2.83 fb
$\sigma(ggA)\text{BR}(A \to ZH_s)$	554.38 fb
$\sigma(ggA)\text{BR}(A \to ZH_s \to bb+A_sA_s \to bb+4\gamma)$	57.36 fb
$\sigma(ggA)\text{BR}(A \to ZH_s \to bb+A_sA_s \to 4b+\gamma\gamma)$	19.99 fb
$\sigma(ggA)\text{BR}(A \to ZH_s \to Z+A_sA_s \to bb+\tau\tau+\gamma\gamma)$	6.35 fb
$\sigma(ggA)\text{BR}(A \to ZH_s \to ll/\tau\tau+A_sA_s \to ll/\tau\tau+4\gamma)$	12.78 fb
$\sigma(ggA)\text{BR}(A \to ZH_s \to ll/\tau\tau+A_sA_s \to ll\tau\tau/4\tau+\gamma\gamma)$	0.42 fb

TABLE IX. The parameters defining scenario B.2, together with the Higgs boson masses, singlet components and reduced signal rates of h.

B.2 (Point ID 1142)	Scenario		
M_h, M_{H_s}, M_H	126.8 GeV	176.2 GeV	556.3 GeV
M_{A_s}, M_A	106.6 GeV	577.8 GeV	
$\lvert S_{H_2h_s}\rvert^2, \lvert P_{A_1a_s}\rvert^2$	0.99	0.92	
$\mu_{\tau\tau}$, μ_{bb}	1.03	1.21	
μ_{ZZ}, μ_{WW}, $\mu_{\gamma\gamma}$	0.93	0.93	0.89
$\tan\beta$, λ, κ	1.61	0.62	−0.22
A_λ, A_κ, μ_{eff}	−709.2 GeV	−169.3 GeV	−236.5 GeV
A_t, A_b, A_τ	−899.8 GeV	−1436.3 GeV	857.5 GeV
M_1, M_2, M_3	651.4 GeV	307.0 GeV	1340.6 GeV
$M_{Q_3} = M_{t_R}$, M_{b_R}	2578.9 GeV	3 TeV	
$M_{L_3} = M_{\tau_R}$, M_{SUSY}	1863.7 GeV	3 TeV	

additionally decays into a lightest neutralino pair at sizeable rate. The trilinear couplings accessible in this scenario are λ_{HH_sh}, λ_{AA_sh} and $\lambda_{AA_sH_s}$.

C. Scenario C - $H_1 \equiv h$ and large $\tan\beta$

Scenario C in Table XIII explicitly features a large value of $\tan\beta$, i.e. $\tan\beta = 17$. Along with this comes a very heavy, additionally practically 100% singletlike, Higgs boson of 3.5 TeV. This makes it very difficult if not impossible to discover the complete NMSSM Higgs spectrum. Due to the large value of $\tan\beta$ gluon fusion is not effective as production mechanism. Instead the signal rates for Higgs production in association with $b\bar{b}$ are given in Table XIV for the doubletlike Higgs bosons H and A, both with masses around 600 GeV, and the singletlike pseudoscalar A_s, that is also rather heavy with a mass around 312 GeV. For comparison we also give the corresponding cross section for the SM-like Higgs boson. The production cross sections are large enough to produce the NMSSM Higgs bosons, apart from the heavy H_s, at sufficient rates for discovery in the standard channels. In addition, the pseudoscalar singlet A_s can be searched for in the cascade decay via $A \to hA_s$ or $H \to ZA_s$. All other Higgs-to-Higgs or Higgs-to-gauge-Higgs decays for H or A are kinematically closed. Therefore in this scenario the only trilinear Higgs coupling that may be measurable is λ_{AA_sh}.

TABLE X. The signal rates for B.2.

B.2 (Point ID 1142)	Signal rates
$\sigma(ggH_s)$	19.03 fb
$\sigma(ggH_s)\text{BR}(H_s \to WW)$	15.46 fb
$\sigma(ggH_s)\text{BR}(H_s \to b\bar{b})$	2.68 fb
$\sigma(ggH_s)\text{BR}(H_s \to \tau\tau)$	0.30 fb
$\sigma(ggH)$	1.15 pb
$\sigma(ggH)\text{BR}(H \to t\bar{t})$	623.39 fb
$\sigma(ggH)\text{BR}(H \to \tilde{\chi}_1^0\tilde{\chi}_1^0)$	10.84 fb
$\sigma(ggH)\text{BR}(H \to ZA_s)$	322.93 fb
$\sigma(ggH)\text{BR}(H \to ZA_s \to ll + b\bar{b})$	9.61 fb
$\sigma(ggH)\text{BR}(H \to ZA_s \to \tau\tau + b\bar{b})$	14.03 fb
$\sigma(ggH)\text{BR}(H \to hH_s)$	26.62 fb
$\sigma(ggH)\text{BR}(H \to hH_s \to \tau\tau + b\bar{b})$	0.50 fb
$\sigma(ggH)\text{BR}(H \to hH_s \to WW + b\bar{b} \to (l\nu)(l\nu)b\bar{b})$	0.16 fb
$\sigma(ggA_s)$	1.56 pb
$\sigma(ggA_s)\text{BR}(A_s \to b\bar{b})$	1.38 pb
$\sigma(ggA_s)\text{BR}(A_s \to \tau\tau)$	140 fb
$\sigma(ggA)$	824.23 fb
$\sigma(ggA)\text{BR}(A \to t\bar{t})$	551.88 fb
$\sigma(ggA)\text{BR}(A \to hA_s)$	184.87 fb
$\sigma(ggA)\text{BR}(A \to hA_s \to bb + bb)$	100.05 fb
$\sigma(ggA)\text{BR}(A \to hA_s \to bb + \tau\tau)$	20.72 fb
$\sigma(ggA)\text{BR}(A \to hA_s \to \tau\tau + \tau\tau)$	1.07 fb
$\sigma(ggA)\text{BR}(A \to hA_s \to bb + \gamma\gamma)$	0.36 fb

D. Scenarios D

The scenarios D are characterized by a SM-like Higgs given by H_2, $H_2 \equiv h$, that can decay into lighter singlet pairs.

TABLE XI. The parameters defining scenario B.3, together with the Higgs boson masses, singlet components and reduced signal rates of h.

B.3 (Point ID 210)	Scenario		
M_h, M_{H_s}, M_H	124.1 GeV	184.3 GeV	463.1 GeV
M_{A_s}, M_A	133.4 GeV	457.2 GeV	
$\lvert S_{H_2h_s}\rvert^2, \lvert P_{A_1a_s}\rvert^2$	0.96	0.99	
$\mu_{\tau\tau}$, μ_{bb}	1.44	1.99	
μ_{ZZ}, μ_{WW}, $\mu_{\gamma\gamma}$	0.90	0.90	0.97
$\tan\beta$, λ, κ	2.22	0.60	0.30
A_λ, A_κ, μ_{eff}	348.7 GeV	4.5 GeV	191.8 GeV
A_t, A_b, A_τ	−1130.2 GeV	−6.5 GeV	1951.6 GeV
M_1, M_2, M_3	136.4 GeV	273.4 GeV	1789.0 GeV
$M_{Q_3} = M_{t_R}$, M_{b_R}	2838.3 GeV	3 TeV	
$M_{L_3} = M_{\tau_R}$, M_{SUSY}	1659.3 GeV	3 TeV	

TABLE XII. The signal rates for B.3.

B.3 (Point ID 210)	Signal rates
$\sigma(ggH_s)$	390.38 fb
$\sigma(ggH_s)\mathrm{BR}(H_s \to b\bar{b})$	160.37 fb
$\sigma(ggH_s)\mathrm{BR}(H_s \to \tau\tau)$	18.46 fb
$\sigma(ggH_s)\mathrm{BR}(H_s \to WW)$	176.63 fb
$\sigma(ggH_s)\mathrm{BR}(H_s \to ZZ)$	29.00 fb
$\sigma(ggH)$	1.326 pb
$\sigma(ggH)\mathrm{BR}(H \to t\bar{t})$	684.96 fb
$\sigma(ggH)\mathrm{BR}(H \to hH_s)$	184.85 fb
$\sigma(ggH)\mathrm{BR}(H \to hH_s \to bb + bb)$	50.46 fb
$\sigma(ggH)\mathrm{BR}(H \to hH_s \to bb + \tau\tau)$	11.08 fb
$\sigma(ggH)\mathrm{BR}(H \to hH_s \to \tau\tau + \tau\tau)$	0.61 fb
$\sigma(ggH)\mathrm{BR}(H \to hH_s \to bb + \gamma\gamma)$	0.24 fb
$\sigma(ggH)\mathrm{BR}(H \to ZA_s)$	36.41 fb
$\sigma(ggH)\mathrm{BR}(H \to ZA_s \to ll + b\bar{b})$	1.09 fb
$\sigma(ggH)\mathrm{BR}(H \to ZA_s \to \tau\tau + b\bar{b})$	1.62 fb
$\sigma(ggA_s)$	31.49 fb
$\sigma(ggA_s)\mathrm{BR}(A_s \to b\bar{b})$	28.03 fb
$\sigma(ggA_s)\mathrm{BR}(A_s \to \tau\tau)$	3.01 fb
$\sigma(ggA_s)\mathrm{BR}(A_s \to \gamma\gamma)$	0.13 fb
$\sigma(ggA)$	1.26 pb
$\sigma(ggA)\mathrm{BR}(A \to t\bar{t})$	680.53 fb
$\sigma(ggA)\mathrm{BR}(A \to \tilde{\chi}_1^0\tilde{\chi}_1^0)$	109.32 fb
$\sigma(ggA)\mathrm{BR}(A \to hA_s)$	31.19 fb
$\sigma(ggA)\mathrm{BR}(A \to hA_s \to b\bar{b} + b\bar{b})$	18.41 fb
$\sigma(ggA)\mathrm{BR}(A \to hA_s \to \tau\tau + b\bar{b})$	3.91 fb
$\sigma(ggA)\mathrm{BR}(A \to hA_s \to \tau\tau + \tau\tau)$	0.21 fb
$\sigma(ggA)\mathrm{BR}(A \to hA_s \to \gamma\gamma + bb)$	0.15 fb
$\sigma(ggA)\mathrm{BR}(A \to H_sA_s)$	20.94 fb
$\sigma(ggA)\mathrm{BR}(A \to H_sA_s \to b\bar{b} + b\bar{b})$	7.67 fb
$\sigma(ggA)\mathrm{BR}(A \to H_sA_s \to \tau\tau + b\bar{b})$	1.71 fb
$\sigma(ggA)\mathrm{BR}(A \to ZH_s)$	90.21 fb
$\sigma(ggA)\mathrm{BR}(A \to ZH_s \to ll + bb)$	1.25 fb
$\sigma(ggA)\mathrm{BR}(A \to ZH_s \to \tau\tau + bb)$	1.90 fb

(D.1) SM-like Higgs decays into light *CP*-even singletlike Higgs pairs: The scenario D.1, Table XV, leads to a very light *CP*-even singlet Higgs H_s with a mass of 9.6 GeV. The branching ratio of the SM-like h, that is copiously produced with a cross section of 44 pb, into H_sH_s makes up 10%. The singlet H_s is so light that it cannot decay into bottom pairs and instead decays at 90% into τ pairs. This leads then to cascade decay rates of 3.6 pb in the decay chain $h \to H_sH_s \to 4\tau$, cf. Table XVI. And even the $(\tau\tau)(\mu\mu)$ final state reaches 32 fb. This channel should therefore not only allow for H_s discovery, but also for the measurement of the triple Higgs coupling $\lambda_{hH_sH_s}$. Better discovery prospects for H_s are obtained in direct gluon fusion production with subsequent decay into e.g. τ pairs. As H_s is so light and not 100% singletlike its gluon fusion cross section is large with 440 pb. The $\tau\tau$ final state rate is then given by enormous 405 pb. And also the rare decays into charm quarks amount to 5.2 pb, allowing for a measurement of the $H_sc\bar{c}$ coupling. The 2γ final state finally reaches 8 fb. The masses of the doublets H and A are around 790 GeV, so that their gluon fusion production cross sections only reach $\mathcal{O}(40\ \mathrm{fb})$. Their masses are large enough so that they decay into top quark pairs, also the lightest neutralino pair final state rates can reach ~6 fb. Furthermore, the branching ratio $\mathrm{BR}(H \to hH_s) = 0.21$ so that the Higgs-to-Higgs cascade into the $(\tau\tau)(b\bar{b})$ final state reaches 4.3 fb and can add to the H_s search channel or alternatively to the measurement of the λ_{HH_sh} coupling. The pseudoscalar can decay via hA_s. However, the $(\tau\tau)(b\bar{b})$ rate is small with 0.3 fb. The extraction of the triple coupling λ_{AA_sh} will be difficult here. But it can add to the A_s discovery, in particular as the gluon fusion cross section for the very singletlike A_s is small. Finally, A can decay into the gauge-Higgs final state ZH_s leading to 1 fb in the $(\tau\tau)(b\bar{b})$ final state.

TABLE XIII. The parameters defining scenario C, together with the Higgs boson masses, singlet components and reduced signal rates of h.

C (Point ID 2296)	Scenario		
M_h, M_H, M_{H_s}	124.1 GeV	597.7 GeV	3528.3 GeV
M_{A_s}, M_A	311.8 GeV	614.5 GeV	
$\lvert S_{H_3h_s}\rvert^2$, $\lvert P_{A_1a_s}\rvert^2$	1	0.93	
$\mu_{\tau\tau}$, μ_{bb}	0.97	1.06	
μ_{ZZ}, μ_{WW}, $\mu_{\gamma\gamma}$	0.78	0.78	0.80
$\tan\beta$, λ, κ	17.06	0.08	−0.63
A_λ, A_κ, μ_{eff}	−1766.2 GeV	−24.2 GeV	−217.1 GeV
A_t, A_b, A_τ	1961.8 GeV	−1535.3 GeV	−1211.9 GeV
M_1, M_2, M_3	478.3 GeV	369.2 GeV	2847.8 GeV
$M_{Q_3} = M_{t_R}$, M_{b_R}	977.0 GeV	3 TeV	
$M_{L_3} = M_{\tau_R}$, M_{SUSY}	2797.1 GeV	3 TeV	

TABLE XIV. The signal rates for C.

C (Point ID 2296)	Higgs decays
$\sigma(bbH)$	346.97 fb
$\sigma(bbH)\mathrm{BR}(H \to b\bar{b})$	190.72 fb
$\sigma(bbH)\mathrm{BR}(H \to \tau\tau)$	23.32 fb
$\sigma(bbH)\mathrm{BR}(H \to t\bar{t})$	5.37 fb
$\sigma(bbH)\mathrm{BR}(H \to \tilde{\chi}_1^0\tilde{\chi}_1^0)$	7.00 fb
$\sigma(bbH)\mathrm{BR}(H \to \tilde{\chi}_1^+\tilde{\chi}_1^-)$	16.21 fb
$\sigma(bbH)\mathrm{BR}(H \to ZA_s)$	101.84 fb
$\sigma(bbH)\mathrm{BR}(H \to ZA_s \to ll + b\bar{b})$	3.08 fb
$\sigma(bbH)\mathrm{BR}(H \to ZA_s \to \tau\tau + b\bar{b})$	4.61 fb
$\sigma(bbA_s)$	404.91 fb
$\sigma(bbA_s)\mathrm{BR}(A_s \to b\bar{b})$	364.21 fb
$\sigma(bbA_s)\mathrm{BR}(A_s \to \tau\tau)$	40.17 fb
$\sigma(bbh)$	643.60 fb
$\sigma(bbA)$	282.80 fb
$\sigma(bbA)\mathrm{BR}(A \to b\bar{b})$	151.41 fb
$\sigma(bbA)\mathrm{BR}(A \to \tau\tau)$	18.60 fb
$\sigma(bbA)\mathrm{BR}(A \to t\bar{t})$	5.08 fb
$\sigma(bbA)\mathrm{BR}(A \to \tilde{\chi}_1^0\tilde{\chi}_1^0)$	6.85 fb
$\sigma(bbA)\mathrm{BR}(A \to hA_s)$	76.27 fb
$\sigma(bbA)\mathrm{BR}(A \to hA_s \to bb + bb)$	46.65 fb
$\sigma(bbA)\mathrm{BR}(A \to hA_s \to bb + \tau\tau)$	9.98 fb
$\sigma(bbA)\mathrm{BR}(A \to hA_s \to \tau\tau + \tau\tau)$	0.53 fb

(D.2) SM-like Higgs decays into light CP-odd singletlike Higgs pairs: In the scenario D.2, defined in Table XVII, the SM-like Higgs can decay into a pair of pseudoscalar singlets A_s. The latter is very light with a mass around 62 GeV. The lightest scalar H_s with a mass of 112 GeV is close in mass to h, and both mix strongly, so that the gluon fusion production cross section for h only amounts to 27 pb, while the H_s production is rather large for a singletlike boson and reaches 17 pb, as given in Table XVIII. The h reduced rates are still compatible with the LHC data, although the final state rates for $\tau\tau$ and $b\bar{b}$ are somewhat on the lower side. The h cascade decay via an A_s pair reaches in the $(\tau\tau)(b\bar{b})$ final state a large cross section of 276 fb. This should make a measurement of the triple Higgs couplings $\lambda_{hA_sA_s}$ possible. Also the 4τ final state is sizeable with 12 fb. The light A_s can be directly produced, too, and then searched for in the $\tau\tau$ final state with a rate of 92 fb. The copiously produced H_s can be searched for in the standard decay channels. Difficult, however, if not impossible is the

TABLE XVI. The signal rates for D.1.

D.1 (Point ID 5416)	Signal rates
$\sigma(ggh)$	44.28 pb
$\sigma(ggh)\mathrm{BR}(h \to H_sH_s)$	4.22 pb
$\sigma(ggh)\mathrm{BR}(h \to H_sH_s \to \tau\tau + \tau\tau)$	3.58 pb
$\sigma(ggh)\mathrm{BR}(h \to H_sH_s \to \tau\tau + \mu\mu)$	31.64 fb
$\sigma(ggH_s)$	439.80 pb
$\sigma(ggH_s)\mathrm{BR}(H_s \to \mu\mu)$	1.79 pb
$\sigma(ggH_s)\mathrm{BR}(H_s \to \tau\tau)$	405.09 pb
$\sigma(ggH_s)\mathrm{BR}(H_s \to c\bar{c})$	5.17 pb
$\sigma(ggH_s)\mathrm{BR}(H_s \to s\bar{s})$	7.24 pb
$\sigma(ggH_s)\mathrm{BR}(H_s \to \gamma\gamma)$	7.95 fb
$\sigma(ggH)$	38.72 fb
$\sigma(ggH)\mathrm{BR}(H \to t\bar{t})$	9.80 fb
$\sigma(ggH)\mathrm{BR}(H \to \tilde{\chi}_1^0\tilde{\chi}_1^0)$	5.73 fb
$\sigma(ggH)\mathrm{BR}(H \to hH_s)$	8.08 fb
$\sigma(ggH)\mathrm{BR}(H \to hH_s \to b\bar{b} + \tau\tau)$	4.26 fb
$\sigma(ggH)\mathrm{BR}(H \to hH_s \to \tau\tau + \tau\tau)$	0.45 fb
$\sigma(ggA_s)$	9.31 fb
$\sigma(ggA_s)\mathrm{BR}(A_s \to b\bar{b})$	3.78 fb
$\sigma(ggA_s)\mathrm{BR}(A_s \to \tau\tau)$	0.46 fb
$\sigma(ggA)$	41.26 fb
$\sigma(ggA)\mathrm{BR}(A \to t\bar{t})$	11.24 fb
$\sigma(ggA)\mathrm{BR}(A \to \tilde{\chi}_1^0\tilde{\chi}_1^0)$	5.94 fb
$\sigma(ggA)\mathrm{BR}(A \to hA_s)$	4.95 fb
$\sigma(ggA)\mathrm{BR}(A \to hA_s \to b\bar{b} + b\bar{b})$	1.15 fb
$\sigma(ggA)\mathrm{BR}(A \to hA_s \to b\bar{b} + \tau\tau)$	0.26 fb
$\sigma(ggA)\mathrm{BR}(A \to ZH_s)$	7.78 fb
$\sigma(ggA)\mathrm{BR}(A \to ZH_s \to b\bar{b} + \tau\tau)$	1.08 fb

TABLE XV. The parameters defining scenario D.1, together with the Higgs boson masses, singlet components and reduced signal rates of h.

D.1 (Point ID 5416)	Scenario		
M_{H_s}, M_h, M_H	9.6 GeV	124.2 GeV	793.4 GeV
M_{A_s}, M_A	273.2 GeV	792.2 GeV	
$\lvert S_{H_1h_s}\rvert^2$, $\lvert P_{A_1A_s}\rvert^2$	0.98	0.99	
$\mu_{\tau\tau}$, μ_{bb}	0.90	0.89	
μ_{ZZ}, μ_{WW}, $\mu_{\gamma\gamma}$	0.92	0.92	0.92
$\tan\beta$, λ, κ	3.37	0.64	0.20
A_λ, A_κ, μ_{eff}	−709.0 GeV	297.3 GeV	−222.4 GeV
A_t, A_b, A_τ	−1075.3 GeV	−1973.1 GeV	−143.7 GeV
M_1, M_2, M_3	307.7 GeV	789.8 GeV	2933.1 GeV
$M_{Q_3} = M_{t_R}$, M_{b_R}	2931.3 GeV	3 TeV	
$M_{L_3} = M_{\tau_R}$, M_{SUSY}	2930.8 GeV	3 TeV	

TABLE XVII. The parameters defining scenario D.2, together with the Higgs boson masses, singlet components and reduced signal rates of h.

D.2 (Point ID 110)	Scenario		
M_{H_s}, M_h, M_H	112.0 GeV	126.3 GeV	1288.2 GeV
M_{A_s}, M_A	61.5 GeV	1287.4 GeV	
$\lvert S_{H_1 h_s}\rvert^2, \lvert P_{A_1 a_s}\rvert^2$	0.63	1	
$\mu_{\tau\tau}$, μ_{bb}	0.73	0.62	
μ_{ZZ}, μ_{WW}, $\mu_{\gamma\gamma}$	0.90	1.03	1.06
$\tan\beta$, λ, κ	6.36	0.47	0.14
A_λ, A_κ, μ_{eff}	1217.1 GeV	19.6 GeV	195.3 GeV
A_t, A_b, A_τ	−1804.6 GeV	−1196.8 GeV	1704.8 GeV
M_1, M_2, M_3	417.2 GeV	237.5 GeV	2362.2 GeV
$M_{Q_3} = M_{t_R}$, M_{b_R}	967.8 GeV	3 TeV	
$M_{L_3} = M_{\tau_R}$, M_{SUSY}	2491.6 GeV	3 TeV	

TABLE XVIII. The signal rates for D.2.

D.2 (Point ID 110)	Signal rates
$\sigma(ggh)$	27.37 pb
$\sigma(ggh)\text{BR}(h \to A_s A_s)$	1.85 pb
$\sigma(ggh)\text{BR}(h \to A_s A_s \to bb + bb)$	1.55 pb
$\sigma(ggh)\text{BR}(h \to A_s A_s \to bb + \tau\tau)$	276.30 fb
$\sigma(ggh)\text{BR}(h \to A_s A_s \to \tau\tau + \tau\tau)$	12.36 fb
$\sigma(ggh)\text{BR}(h \to A_s A_s \to bb + \gamma\gamma)$	0.34 fb
$\sigma(ggH_s)$	17.25 pb
$\sigma(ggH_s)\text{BR}(H_s \to b\bar{b})$	14.64 pb
$\sigma(ggH_s)\text{BR}(H_s \to \tau\tau)$	1.50 pb
$\sigma(ggH_s)\text{BR}(H_s \to \gamma\gamma)$	13.93 fb
$\sigma(ggH_s)\text{BR}(H_s \to ZZ)$	23.90 fb
$\sigma(ggH_s)\text{BR}(H_s \to WW)$	401.21 fb
$\sigma(ggH_s)\text{BR}(H_s \to \mu\mu)$	5.33 fb
$\sigma(ggH_s)\text{BR}(H_s \to Z\gamma)$	4.15 fb
$\sigma(ggA_s)$	1.13 pb
$\sigma(ggA_s)\text{BR}(A_s \to b\bar{b})$	1.03 pb
$\sigma(ggA_s)\text{BR}(A_s \to \tau\tau)$	92.46 fb
$\sigma(ggH)$	0.46 fb
$\sigma(bbH)$	0.82 fb
$\sigma(ggA)$	0.72 fb
$\sigma(bbA)$	0.82 fb

production of the doubletlike H and A, as they have masses of 1.3 TeV. Since they are both rather down-component doubletlike, one might consider associated production with a b-quark pair, in view of the not so small $\tan\beta = 6.4$. But also these cross sections remain below 1 fb.

Picking up the idea presented in [97], sum rules for the Higgs couplings can be exploited to give a hint to the missing states, in case the heavy Higgs bosons cannot be discovered. This allows then to disentangle an NMSSM Higgs sector from a supersymmetric Higgs sector with minimal particle content, if e.g. only three Higgs bosons are discovered and not all of them are scalar. From Eq. (4.3) and the unitarity of the $\mathcal{R}^S$ matrix, it can be derived that the NMSSM CP-even Higgs couplings to vector bosons with respect to the SM coupling obey the sum rule

$$\sum_{i=1}^{3} g^2_{H_i VV} = 1. \tag{6.1}$$

The H_i couplings $G_{H_i tt/bb}$ to top and bottom quarks (normalized to the SM) are given by

$$\frac{G_{H_i tt}}{g_{H^{\text{SM}} tt}} \equiv g_{H_i tt} = \frac{\mathcal{R}^S_{i2}}{\sin\beta} \tag{6.2}$$

$$\frac{G_{H_i bb}}{g_{H^{\text{SM}} bb}} \equiv g_{H_i bb} = \frac{\mathcal{R}^S_{i1}}{\cos\beta}. \tag{6.3}$$

Exploiting the unitarity of $\mathcal{R}^S$ leads to the sum rule

$$\frac{1}{\sum_{i=1}^{3} g^2_{H_i tt}} + \frac{1}{\sum_{i=1}^{3} g^2_{H_i bb}} = 1. \tag{6.4}$$

If three neutral Higgs bosons are discovered, but not all of them are CP-even, then these rules are violated, while in the MSSM with only three neutral Higgs bosons in total the sum rules would be fulfilled. Applying this to our scenario, in case among the CP-even Higgs bosons we only find h and H_s but not the heavy H, the sums Eqs. (6.1) and (6.4) result in

$$\sum_{i=1}^{2} g^2_{H_i VV} \approx 1 \tag{6.5}$$

for the gauge couplings and

$$\frac{1}{\sum_{i=1}^{2} g^2_{H_i tt}} + \frac{1}{\sum_{i=1}^{2} g^2_{H_i bb}} = 1.85 \tag{6.6}$$

for the Yukawa couplings. As the heavy doublet H is dominated by the H_d component $\mathcal{R}^S_{31}$ and the coupling to down-type quarks is additionally enhanced for large $\tan\beta$ values, cf. Eq. (6.3), the missing H_3 coupling to down-type quarks has a large effect on the Yukawa coupling sum rule.

For the same reason the effect on the vector coupling sum rule is negligible, cf. Eq. (4.3). At a future high-energy LHC the couplings to fermions will be measurable at $\mathcal{O}(10\text{–}20\%)$ level accuracy [98]. This is largely sufficient to test for the deviation in the Yukawa coupling sum rule in this scenario.

VII. CONCLUSIONS

After the discovery of the Higgs boson at the LHC no direct sign of new particles beyond the SM has shown up yet. Also the discovered Higgs boson itself looks very SM-like. Still it could be the SM-like resonance of an extended Higgs sector as it emerges in supersymmetric theories. In particular, the NMSSM with five neutral Higgs bosons gives rise to a very interesting phenomenology and a plethora of new signatures. We have investigated in a large scan over the NMSSM parameter range, what the prospects of pinning down the NMSSM Higgs sector at the 13 TeV run of the LHC are. Hereby we have taken into account the constraints that arise from the LEP, Tevatron and LHC Higgs boson searches, from dark matter measurements and low-energy observables and from exclusion bounds on SUSY particles. We find, that in the NMSSM both the lightest or next-to-lightest Higgs boson can be the SM-like Higgs boson. The LHC Higgs signal can also be built up by two Higgs resonances that are almost degenerate and have masses close to 125 GeV. Furthermore, viable scenarios can be found for low and high $\tan\beta$ values.

We have investigated the production rates of the neutral Higgs bosons in the SM final states. A lot of scenarios should be accessible at the LHC, some, however, will be challenging and possibly not allow for the discovery of all NMSSM Higgs bosons. We therefore subsequently focused on the subspace of the NMSSM, that we call the natural NMSSM, and which features heavy Higgs bosons with masses below about 530 GeV and besides a light CP-odd singlet state a light CP-even singletlike Higgs boson with a mass between about 62 and 117 GeV. The study of the signal rates in the SM final states reveals that the natural NMSSM should give access to all neutral NMSSM Higgs bosons in most of the scenarios. Where the discovery in direct production is difficult, it can be complemented by searches in Higgs-to-Higgs or Higgs-to-gauge boson-Higgs decays. It should therefore be possible to discover the natural NMSSM Higgs bosons at the next run of the LHC or to strongly constrain this scenario.

Higgs decays into Higgs pairs offer an interesting alternative to the discovery of Higgs states that may be difficult to be accessed in direct production. At the same time they give access to the trilinear Higgs self-coupling involved in the Higgs-to-Higgs decays. Taking the results of our large parameter scan we have extracted benchmark scenarios that highlight different properties of Higgs-to-Higgs-decays. In analysing the various decay signatures, we found multiphoton and multifermion signatures that not only lead to very promising signal rates (far above the ones to be expected in SM Higgs pair production), but some of them are also unique to the NMSSM and lead to spectacular final states with up to six photons. Another interesting outcome is the possibility of CP-even singlet states that are below the bottom pair threshold, so that the decays into other light fermions are dominant and give access to the measurement of Higgs couplings to taus, muons and even light quarks. Finally, we show in one example, how coupling measurements could help to point to an additional CP-even Higgs boson, in case not all CP-even states should have been discovered.

In summary, our results show that the search for Higgs bosons needs to be continued not only in the high- but also in the low-mass regions below 125 GeV. Furthermore, we have to be prepared for new exotic signatures that cannot appear in minimal supersymmetric extensions of the SM, but are possible in the NMSSM due to significant signal rates arising from Higgs pair production in Higgs decays.

ACKNOWLEDGMENTS

We thank Alexander Nikitenko and Markus Schumacher for fruitful discussions and advise. R. N. also thanks Peter Athron, Anthony Thomas and Anthony Williams for useful discussions. M. M. acknowledges discussions with Conny Beskidt, Ramona Gröber, Rui Santos and Michael Spira. M. M. is supported by the DFG SFB/TR9 "Computational Particle Physics". The work by R. N. was supported by the Australian Research Council through the ARC Center of Excellence in Particle Physics at the Terascale. S. F. K. is supported by the STFC Consolidated Grant No. ST/J000396/1 and EU ITN Grant No. INVISIBLES 289442. K. W. gratefully acknowledges support of the Graduiertenkolleg GRK1694 "Elementarteilchen bei höchster Energie und höchster Präzision".

APPENDIX: HIGGS COUPLINGS IN THE NATURAL NMSSM

In the following approximations for the Higgs couplings in the parameter range of the natural NMSSM will be given. First of all, the 125 GeV Higgs boson has to be produced with SM-like rates. This means that it must have large enough couplings to top quarks and hence a large H_u component. At the same time, it is advantageous not to have a too large H_d component, as then the coupling to b quarks is suppressed, leading to enhanced branching ratios that account for a possible slight suppression in the production. Due to the unitarity of the mixing matrix rotating the interaction to the Higgs mass eigenstates, this means, that the other doubletlike heavier Higgs boson must be H_d-like. The light CP-even and CP-odd Higgs bosons, H_s and A_s respectively, must be singletlike in order to avoid the exclusion bounds. In summary, for the natural NMSSM the approximate compositions of the CP-even Higgs mass eigenstates expressed in terms of the mixing matrix $\mathcal{R}_{ij}$ ($i = H_s, h, H, j = h_d, h_u, h_s$), in the notation of Section V, are given by

$$(H_s, h, H)^T = \mathcal{R}^S (h_d, h_u, h_s)^T = \begin{pmatrix} 0 & 0 & 1 \\ 0 & 1 & 0 \\ 1 & 0 & 0 \end{pmatrix} (h_d, h_u, h_s)^T. \quad \text{(A1)}$$

For the composition of the pseudoscalars we have,

$$(A_s, A)^T = \mathcal{R}^P (a, a_s)^T = \begin{pmatrix} 0 & 1 \\ 1 & 0 \end{pmatrix} (a, a_s)^T, \quad \text{(A2)}$$

with $a = \sin\beta a_d + \cos\beta a_u$. Comparing this with the actual composition as result of our scan, the actual composition is approximated rather well, with at most 30% deviations. With these assumptions we get for the trilinear Higgs couplings involved in the Higgs-to-Higgs decays, in units of the SM coupling,

$$g_{Hhh} = \frac{\cos\beta}{M_Z^2}(\lambda^2 v^2 - M_Z^2) \quad \text{(A3)}$$

$$g_{HhH_s} = \frac{-v}{\sqrt{2}M_Z^2}(\lambda A_\lambda + 2\kappa\mu) \quad \text{(A4)}$$

$$g_{HH_sH_s} = \frac{\lambda v^2}{M_Z^2}(\lambda\cos\beta - \kappa\sin\beta) \quad \text{(A5)}$$

$$g_{hH_sH_s} = \frac{\lambda v^2}{M_Z^2}(\lambda\sin\beta - \kappa\cos\beta) \quad \text{(A6)}$$

$$g_{hAA_s} = \frac{\lambda v\sin\beta}{2M_Z^2}(\sqrt{2}A_\lambda - 2\kappa v_s) \quad \text{(A7)}$$

$$g_{hA_sA_s} = \frac{\lambda v^2}{M_Z^2}(\kappa\cos\beta + \lambda\sin\beta) \quad \text{(A8)}$$

$$g_{H_sAA_s} = \frac{-\lambda v^2\kappa}{M_Z^2} \quad \text{(A9)}$$

$$g_{HA_sA_s} = \frac{\lambda v^2}{M_Z^2}(\kappa\sin\beta + \lambda\cos\beta). \quad \text{(A10)}$$

[1] G. Aad *et al.* (ATLAS Collaboration), Phys. Lett. B **716**, 1 (2012); Report No. ATLAS-CONF-2012-162.

[2] S. Chatrchyan *et al.* (CMS Collaboration), Phys. Lett. B **716**, 30 (2012); Report No. CMS-PAS-HIG-12-045.

[3] D. V. Volkov and V. P. Alkulov, Phys. Lett. **46B**, 109 (1973); J. Wess and B. Zumino, Nucl. Phys. **B70**, 39 (1974); P. Fayet, Phys. Lett. **64B**, 159 (1976); **69B**, 489 (1977); **84B**, 416 (1979); G. F. Farrar and P. Fayet, Phys. Lett. **76B**, 575 (1978); S. Dimopoulos and H. Georgi, Nucl. Phys. **B193**, 150 (1981); N. Sakai, Z. Phys. C **11**, 153 (1981); E. Witten, Nucl. Phys. **B188**, 513 (1981); H. P. Nilles, Phys. Rep. **110**, 1 (1984); H. E. Haber and G. L. Kane, Phys. Rep. **117**, 75 (1985); M. F. Sohnius, Phys. Rep. **128**, 39 (1985); J. F. Gunion and H. E. Haber, Nucl. Phys. **B272**, 1 (1986); **B402**, 567(E) (1993); **B278**, 449 (1986); A. B. Lahanas and D. V. Nanopoulos, Phys. Rep. **145**, 1 (1987).

[4] For reviews and further references, see J. F. Gunion, H. E. Haber, G. Kane, and S. Dawson, *The Higgs Hunter's Guide* (Addison-Wesley, Reading, MA, 1990); S. P. Martin, Adv. Ser. Dir. High Energy Phys. **21**, 1 (2010); S. Dawson, arXiv: hep-ph/9712464; M. Gomez-Bock, M. Mondragon, M. Mühlleitner, R. Noriega-Papaqui, I. Pedraza, M. Spira, and P. M. Zerwas, J. Phys. Conf. Ser. **18**, 74 (2005); M. Gomez-Bock, M. Mondragon, M. Mühlleitner, M. Spira, and P. M. Zerwas, arXiv:0712.2419; A. Djouadi, Phys. Rept. **459**, 1 (2008).

[5] P. Fayet, Nucl. Phys. **B90**, 104 (1975); R. Barbieri, S. Ferrara, and C. A. Savoy, Phys. Lett. **119B**, 343 (1982); M. Dine, W. Fischler, and M. Srednicki, Phys. Lett. **104B**, 199 (1981); H. P. Nilles, M. Srednicki, and D. Wyler, Phys. Lett. **120B**, 346 (1983); J. M. Frere, D. R. T. Jones, and S. Raby, Nucl. Phys. **B222**, 11 (1983); J. P. Derendinger and C. A. Savoy, Nucl. Phys. **B237**, 307 (1984); J. R. Ellis, J. F. Gunion, H. E. Haber, L. Roszkowski, and F. Zwirner, Phys. Rev. D **39**, 844 (1989); M. Drees, Int. J. Mod. Phys. A **04**, 3635 (1989); U. Ellwanger, M. Rausch de Traubenberg, and C. A. Savoy, Phys. Lett. B **315**, 331 (1993); Z. Phys. C **67**, 665 (1995); Nucl. Phys. **B492**, 21 (1997); T. Elliott, S. F. King, and P. L. White, Phys. Lett. B **351**, 213 (1995); S. F. King and P. L. White, Phys. Rev. D **52**, 4183 (1995); F. Franke and H. Fraas, Int. J. Mod. Phys. A **12**, 479 (1997); M. Maniatis, Int. J. Mod. Phys. A **25**, 3505 (2010); U. Ellwanger, C. Hugonie, and A. M. Teixeira, Phys. Rep. **496**, 1 (2010).

[6] J. E. Kim and H. P. Nilles, Phys. Lett. **138B**, 150 (1984).

[7] M. Bastero-Gil, C. Hugonie, S. F. King, D. P. Roy, and S. Vempati, Phys. Lett. B **489**, 359 (2000); A. Delgado, C. Kolda, J. P. Olson, and A. de la Puente, Phys. Rev. Lett. **105**, 091802 (2010); U. Ellwanger, G. Espitalier-Noel, and C. Hugonie, J. High Energy Phys. 09 (2011) 105; G. G. Ross and K. Schmidt-Hoberg, Nucl. Phys. **B862**, 710 (2012); L. J. Hall, D. Pinner, and J. T. Ruderman, J. High Energy Phys. 04 (2012) 131; Z. Kang, J. Li, and T. Li, J. High Energy Phys. 11 (2012) 024; J.-J. Cao, Z.-X. Heng, J. M. Yang, Y.-M. Zhang, and J.-Y. Zhu, J. High Energy Phys. 03 (2012) 086; J. Cao, Z. Heng, J. M. Yang, and J. Zhu, J. High Energy Phys. 10 (2012) 079; J. R. Espinosa, C. Grojean, V. Sanz, and M. Trott, J. High Energy Phys. 12 (2012) 077; M. Perelstein and B. Shakya, Phys. Rev. D **88**, 075003 (2013); K. Agashe, Y. Cui, and R. Franceschini, J. High Energy Phys. 02 (2013) 031.

[8] S. F. King, M. Muhlleitner, and R. Nevzorov, Nucl. Phys. **B860**, 207 (2012); S. F. King, M. Muhlleitner, R. Nevzorov, and K. Walz, Nucl. Phys. **B870**, 323 (2013).

[9] S. Schael *et al.* (ALEPH, DELPHI, L3, and OPAL Collaborations), Eur. Phys. J. C **47**, 547 (2006).
[10] D. T. Nhung, M. Muhlleitner, J. Streicher, and K. Walz, J. High Energy Phys. 11 (2013) 181.
[11] U. Ellwanger, J. High Energy Phys. 08 (2013) 077.
[12] S. Munir, Phys. Rev. D **89**, 095013 (2014).
[13] U. Ellwanger, Phys. Lett. B **698**, 293 (2011); J. High Energy Phys. 03 (2012) 044; A. Arvanitaki and G. Villadoro, J. High Energy Phys. 02 (2012) 144.
[14] J. F. Gunion, Y. Jiang, and S. Kraml, Phys. Rev. D **86**, 071702 (2012).
[15] J. F. Gunion, Y. Jiang, and S. Kraml, Phys. Rev. Lett. **110**, 051801 (2013).
[16] U. Ellwanger, Phys. Lett. B **303**, 271 (1993); T. Elliott, S. F. King, and P. L. White, Phys. Lett. B **305**, 71 (1993); **314**, 56 (1993); Phys. Rev. D **49**, 2435 (1994); P. N. Pandita, Z. Phys. C **59**, 575 (1993); Phys. Lett. B **318**, 338 (1993).
[17] U. Ellwanger and C. Hugonie, Phys. Lett. B **623**, 93 (2005).
[18] G. Degrassi and P. Slavich, Nucl. Phys. **B825**, 119 (2010).
[19] F. Staub, W. Porod, and B. Herrmann, J. High Energy Phys. 10 (2010) 040.
[20] K. Ender, T. Graf, M. Mühlleitner, and H. Rzehak, Phys. Rev. D **85**, 075024 (2012).
[21] S. W. Ham, J. Kim, S. K. Oh, and D. Son, Phys. Rev. D **64**, 035007 (2001); S. W. Ham, S. H. Kim, S. K. Oh, and D. Son, Phys. Rev. D **76**, 115013 (2007).
[22] S. W. Ham, S. K. Oh, and D. Son, Phys. Rev. D **65**, 075004 (2002); S. W. Ham, Y. S. Jeong, and S. K. Oh, arXiv:hep-ph/0308264.
[23] K. Funakubo and S. Tao, Prog. Theor. Phys. **113**, 821 (2005).
[24] T. Graf, R. Grober, M. Muhlleitner, H. Rzehak, and K. Walz, J. High Energy Phys. 10 (2012) 122.
[25] K. Cheung, T.-J. Hou, J. S. Lee, and E. Senaha, Phys. Rev. D **82**, 075007 (2010).
[26] U. Ellwanger, J. F. Gunion, and C. Hugonie, J. High Energy Phys. 02 (2005) 066; U. Ellwanger and C. Hugonie, Comput. Phys. Commun. **175**, 290 (2006).
[27] U. Ellwanger and C. Hugonie, Comput. Phys. Commun. **177**, 399 (2007); see also, G. Chalons and F. Domingo, Phys. Rev. D **86**, 115024 (2012).
[28] J. Baglio, R. Grober, M. Muhlleitner, D. T. Nhung, H. Rzehak, M. Spira, J. Streicher, and K. Walz, arXiv:1312.4788.
[29] Z. Kang, J. Li, T. Li, D. Liu, and J. Shu, Phys. Rev. D **88**, 015006 (2013).
[30] D. G. Cerdeno, P. Ghosh, and C. B. Park, J. High Energy Phys. 06 (2013) 031.
[31] M. Badziak, M. Olechowski, and S. Pokorski, J. High Energy Phys. 06 (2013) 043.
[32] S. Munir, L. Roszkowski, and S. Trojanowski, Phys. Rev. D **88**, 055017 (2013).
[33] D. G. Cerdeno, P. Ghosh, C. B. Park, and M. Peiro, J. High Energy Phys. 02 (2014) 048.
[34] C. Beskidt, W. de Boer, and D. I. Kazakov, Phys. Lett. B **726**, 758 (2013).
[35] K. Choi, S. H. Im, K. S. Jeong, and M.-S. Seo, J. High Energy Phys. 01 (2014) 072.
[36] J. Kozaczuk and S. Profumo, Phys. Rev. D **89**, 095012 (2014).
[37] J. Cao, F. Ding, C. Han, J. M. Yang, and J. Zhu, J. High Energy Phys. 11 (2013) 018.
[38] J.-W. Fan, J.-Q. Tao, Y.-Q. Shen, G.-M. Chen, H.-S. Chen, S. Gascon-Shotkin, M. Lethuillier, L. Sgandurra, and P. Soulet, Chin. Phys. C **38**, 073101 (2014).
[39] J. Huang, T. Liu, L.-T. Wang, and F. Yu, Phys. Rev. Lett. **112**, 221803 (2014).
[40] G. Belanger, V. Bizouard, and G. Chalons, Phys. Rev. D **89**, 095023 (2014).
[41] C. Beskidt, W. de Boer, and D. I. Kazakov, arXiv:1402.4650.
[42] D. Buttazzo, arXiv:1405.3321.
[43] U. Ellwanger and C. Hugonie, arXiv:1405.6647.
[44] U. Ellwanger and A. M. Teixeira, arXiv:1406.7221.
[45] R. D. Peccei and H. R. Quinn, Phys. Rev. Lett. **38**, 1440 (1977); Phys. Rev. D **16**, 1791 (1977).
[46] A. Djouadi, M. Spira, and P. M. Zerwas, Phys. Lett. B **264**, 440 (1991); Z. Phys. C **70**, 427 (1996); M. Spira, A. Djouadi, D. Graudenz, and R. M. Zerwas, Nucl. Phys. **B453**, 17 (1995); A. Djouadi, J. Kalinowski, and M. Spira, Comput. Phys. Commun. **108**, 56 (1998); J. M. Butterworth, A. Arbey, L. Basso, S. Belov, A. Bharucha, F. Braam, A. Buckley, and M. Campanelli *et al.*, arXiv:1003.1643.
[47] A. Djouadi, M. M. Muhlleitner, and M. Spira, Acta Phys. Polon. B **38**, 635 (2007).
[48] D. Das, U. Ellwanger, and A. M. Teixeira, Comput. Phys. Commun. **183**, 774 (2012).
[49] M. Muhlleitner, A. Djouadi, and Y. Mambrini, Comput. Phys. Commun. **168**, 46 (2005); M. Muhlleitner, Acta Phys. Polon. B **35**, 2753 (2004).
[50] P. Z. Skands *et al.*, J. High Energy Phys. 07 (2004) 036; B. C. Allanach *et al.*, Comput. Phys. Commun. **180**, 8 (2009).
[51] ATLAS Collaboration, Report No. ATLAS-CONF-2013-090; CMS Collaboration, Report No. CMS-PAS-HIG-12-052.
[52] G. Aad *et al.* (ATLAS Collaboration), arXiv:1405.7875; Eur. Phys. J. C **72**, 2237 (2012); Phys. Lett. B **720**, 13 (2013); J. High Energy Phys. 06 (2014) 124; J. High Energy Phys. 10 (2013) 189; arXiv:1407.0583; J. High Energy Phys. 09 (2014) 015.
[53] G. Aad *et al.* (ATLAS Collaboration), Phys. Rev. D**90**, 052008 (2014).
[54] CMS Collaboration, CMS-PAS-SUS-13-019; Report No. CMS-PAS-SUS-13-024; Report No. CMS-PAS-SUS-14-011; Report No. CMS-PAS-SUS-13-011; Report No. CMS-PAS-SUS-13-004; Report No. CMS-PAS-SUS-13-014; Report No. CMS-PAS-SUS-13-018; Report No. CMS-PAS-SUS-13-008; Report No. CMS-PAS-SUS-13-013.
[55] G. Belanger, F. Boudjema, A. Pukhov, and A. Semenov, Comput. Phys. Commun. **149**, 103 (2002); Comput. Phys. Commun. **174**, 577 (2006); Comput. Phys. Commun. **180**, 747 (2009); G. Bélanger, F. Boudjema, P. Brun, A. Pukhov, S. Rosier-Lees, P. Salati, and A. Semenov, Comput. Phys. Commun. **182**, 842 (2011).
[56] P. A. R. Ade *et al.* (Planck Collaboration), arXiv:1303.5076.
[57] ATLAS Collaboration, ATLAS-CONF-2012-168; CMS Collaboration, Report No. CMS-PAS-HIG-13-001.
[58] ATLAS Collaboration, ATLAS-CONF-2013-013; CMS Collaboration, Report No. CMS-PAS-HIG-13-002.

[59] ATLAS Collaboration, Report No. ATLAS-CONF-2013-030; CMS Collaboration, Report No. CMS-PAS-HIG-13-003.
[60] ATLAS Collaboration, Report No. ATLAS-CONF-2012-161; CMS Collaboration, Report No. CMS-PAS-HIG-12-044.
[61] ATLAS Collaboration, Report No. ATLAS-CONF-2012-160; CMS Collaboration, Report No. CMS-PAS-HIG-13-004.
[62] ATLAS Collaboration, Report No. ATLAS-CONF-2013-009; CMS CollaborationReport No. CMS-PAS-HIG-13-006.
[63] ATLAS Collaboration, Report No. ATLAS-CONF-2013-010.
[64] D. Graudenz, M. Spira, and P. M. Zerwas, Phys. Rev. Lett. **70**, 1372 (1993); M. Spira, A. Djouadi, D. Graudenz, and P. M. Zerwas, Phys. Lett. B **318**, 347 (1993); Nucl. Phys. **B453**, 17 (1995).
[65] R. V. Harlander and W. B. Kilgore, Phys. Rev. Lett. **88**, 201801 (2002); C. Anastasiou and K. Melnikov, Nucl. Phys. **B646**, 220 (2002); V. Ravindran, J. Smith, and W. L. van Neerven, Nucl. Phys. **B665**, 325 (2003).
[66] S. Marzani, R. D. Ball, V. Del Duca, S. Forte, and A. Vicini, Nucl. Phys. B, Proc. Suppl. **186**, 98 (2009); R. V. Harlander and K. J. Ozeren, J. High Energy Phys. 11 (2009) 088; A. Pak, M. Rogal, and M. Steinhauser, J. High Energy Phys. 02 (2010) 025; R. V. Harlander, H. Mantler, S. Marzani, and K. J. Ozeren, Eur. Phys. J. C **66**, 359 (2010); A. Pak, M. Rogal, and M. Steinhauser, J. High Energy Phys. 09 (2011) 088.
[67] S. Catani, D. de Florian, M. Grazzini, and P. Nason, J. High Energy Phys. 07 (2003) 028.
[68] V. Ravindran, Nucl. Phys. **B746**, 58 (2006); **B752**, 173 (2006).
[69] S. Moch and A. Vogt, Phys. Lett. B **631**, 48 (2005); R. D. Ball, M. Bonvini, S. Forte, S. Marzani, and G. Ridolfi, Nucl. Phys. **B874**, 746 (2013).
[70] G. L. Kane, G. D. Kribs, S. P. Martin, and J. D. Wells, Phys. Rev. D **53**, 213 (1996); S. Dawson, A. Djouadi, and M. Spira, Phys. Rev. Lett. **77**, 16 (1996); A. Djouadi, Phys. Lett. B **435**, 101 (1998); C. Anastasiou, S. Beerli, S. Bucherer, A. Daleo, and Z. Kunszt, J. High Energy Phys. 01 (2007) 082; U. Aglietti, R. Bonciani, G. Degrassi, and A. Vicini, J. High Energy Phys. 01 (2007) 021; M. Muhlleitner and M. Spira, Nucl. Phys. **B790**, 1 (2008); A. Arvanitaki and G. Villadoro, J. High Energy Phys. 02 (2012) 144.
[71] M. Spira, Fortschr. Phys. **46**, 203 (1998).
[72] M. Spira, arXiv:hep-ph/9510347; Nucl. Instrum. Methods Phys. Res., Sect. A **389**, 357 (1997).
[73] A. Djouadi and P. Gambino, Phys. Rev. Lett. **73**, 2528 (1994); U. Aglietti, R. Bonciani, G. Degrassi, and A. Vicini, Phys. Lett. B **595**, 432 (2004); G. Degrassi and F. Maltoni, Phys. Lett. B **600**, 255 (2004); S. Actis, G. Passarino, C. Sturm, and S. Uccirati, Phys. Lett. B **670**, 12 (2008); C. Anastasiou, R. Boughezal, and F. Petriello, J. High Energy Phys. 04 (2009) 003.
[74] ATLAS Collaboration, Report No. ATLAS-CONF-2013-034.
[75] CMS Collaboration, Report No. CMS-PAS-HIG-13-005.
[76] J. R. Espinosa, M. Muhlleitner, C. Grojean, and M. Trott, J. High Energy Phys. 09 (2012) 126.
[77] D. J. Miller, R. Nevzorov, and P. M. Zerwas, Nucl. Phys. **B681**, 3(2004).
[78] ATLAS Collaboration, Report No. ATLAS-CONF-2013-068.
[79] CMS Collaboration, Report No. CMS-PAS-SUS-13-009.
[80] V. M. Abazov *et al.* (D0 Collaboration), Phys. Lett. B **665**, 1 (2008); T. Aaltonen *et al.* (CDF Collaboration), J. High Energy Phys. 10 (2012) 158.
[81] G. Abbiendi *et al.* (OPAL Collaboration), Phys. Lett. B **456**, 95 (1999); **545**, 272 (2002); **548**, 258(E) (2002).
[82] C. Boehm, A. Djouadi, and Y. Mambrini, Phys. Rev. D **61**, 095006 (2000).
[83] A. Delgado, G. F. Giudice, G. Isidori, M. Pierini, and A. Strumia, Eur. Phys. J. C **73**, 2370 (2013).
[84] G. Aad *et al.* (ATLAS Collaboration), arXiv:1407.0583.
[85] K. I. Hikasa and M. Kobayashi, Phys. Rev. D **36**, 724 (1987).
[86] M. Muhlleitner and E. Popenda, J. High Energy Phys. 04 (2011) 095.
[87] Y. Grossman, Z. 'e. Surujon, and J. Zupan, J. High Energy Phys. 03 (2013) 176.
[88] R. V. Harlander, S. Liebler, and H. Mantler, Comput. Phys. Commun. **184**, 1605 (2013).
[89] ATLAS Collaboration, Report Nos. ATLAS-TDR-15 and CERN-LHCC-99-015.
[90] S. Dittmaier *et al.* (LHC Higgs Cross Section Working Group Collaboration), arXiv:1101.0593.
[91] S. Chatrchyan *et al.* (CMS Collaboration), Phys. Rev. Lett. **109**, 121801 (2012).
[92] ATLAS Collaboration, Report No. ATLAS-CONF-2012-079.
[93] CMS Collaboration, Report No. CMS-PAS-HIG-13-032.
[94] G. Aad *et al.* (ATLAS Collaboration), arXiv:1406.5053.
[95] R. Nevzorov and D. J. Miller, arXiv:hep-ph/0411275.
[96] A. Djouadi, W. Kilian, M. Muhlleitner, and P. M. Zerwas, Eur. Phys. J. C **10**, 27 (1999); **10**, 45 (1999); M. M. Muhlleitner, arXiv:hep-ph/0008127.
[97] C. Englert, A. Freitas, M. Muhlleitner, T. Plehn, M. Rauch, M. Spira, and K. Walz, J. Phys. G **41**, 113001 (2014).
[98] CMS Collaboration, arXiv:1307.7135; ATLAS Collaboration, arXiv:1307.7292; S. Dawson, A. Gritsan, H. Logan, J. Qian, C. Tully, R. Van Kooten, A. Ajaib, and A. Anastassov *et al.*, arXiv:1310.8361.